Agricultural and Forest Meteorology 370 (2025) 110597

Contents lists available at ScienceDirect

Agricultural and Forest Meteorology

journal homepage: www.elsevier.com/locate/agrformet

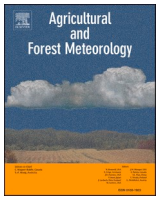

When do clouds and aerosols lead to higher canopy photosynthesis?

Kevin H.H. van Diepen [a,b,*], Elias Kaiser [b,1], Oscar K. Hartogensis [a], Alexander Graf [c], Jordi Vilà-Guerau de Arellano [a,d], Arnold F. Moene [a]

[a] Meteorology and Air Quality Section, Wageningen University, 6708PB Wageningen, the Netherlands
[b] Horticulture and Product Physiology Group, Wageningen University, 6700 AA Wageningen, the Netherlands
[c] Institute of Bio- and Geosciences, IBG-3, Agrosphere, Forschungszentrum Jülich GmbH, 52425 Jülich, Germany
[d] Atmospheric Chemistry Department, Max Planck Institute for Chemistry, 55128 Mainz, Germany

ARTICLE INFO

Keywords:
Canopy photosynthesis
Solar radiation
Diffuse radiation
Diffuse fertilization effect
Clouds
Aerosols
Carbon cycle

ABSTRACT

Clouds and aerosols can increase canopy photosynthesis relative to clear-sky values through changes in total and diffuse solar radiation: the diffuse fertilization effect (DFE). DFE varies across observational sites due to (a) inconsistent definitions and quantifications of DFE, (b) unexplored relationships between DFE and cloudiness type, and (c) insufficient knowledge of the effect of site characteristics. We showed that: DFE definitions vary, DFE quantifications do not connect to existing definitions or do not isolate the causal factor, and a systematic protocol to quantify DFE is lacking. A new theoretical framework served to clarify the relation between DFE definitions, and showed how DFE varies with cloudiness types and site characteristics. We proposed guidelines for a systematic DFE quantification across studies, and which aim to isolate the causal factor of DFE.

Applying our framework to observations of canopy photosynthesis, solar radiation and cloudiness types we quantified DFE at daily and sub-daily time scales. We showed for the first time how DFE varies with cloudiness type, due to the varying trade-off between diffuse radiation and total solar radiation. Using an observation-driven canopy photosynthesis model, we showed that the DFE varies with site characteristics and time of day. The DFE responded strongly to leaf area index, canopy nitrogen distribution, leaf orientation and leaf transmittance, with leaf area index and leaf orientation driving DFE occurrences at our site. Our study emphasizes the importance of quantifying the DFE systematically and accurately across observational sites and highlights the need for information on cloudiness climatology and site characteristics.

1. Introduction

A major determinant of canopy photosynthesis (A_{can}) is the amount of solar radiation reaching the land surface, a fact that has been known for over two centuries (Geerdt, 2007; Gest, 2000; Ingenhousz, 1779). Since the early nineties, A_{can} has been observed to be sensitive to the geometry of solar radiation as well (Denmead, 1991; Price and Black, 1990): when traversing the atmosphere, solar radiation may be scattered through interactions with molecules, aerosols or clouds, and thus made diffuse. Diffuse radiation arrives from all directions compared to non-scattered (direct) radiation, and is more evenly distributed among the leaves in a canopy. Since leaf photosynthesis rate saturates at high levels of solar radiation (i.e. decreasing slope of photosynthesis vs. solar radiation), a more even radiation distribution increases radiation use efficiency (Roderick et al., 2001). Clouds and aerosols can therefore push A_{can} above clear-sky rates, a phenomenon known as the diffuse fertilization effect (DFE)(Kanniah et al., 2012). The occurrence of this phenomenon is not guaranteed, however, since clouds and aerosols also attenuate solar radiation, thus reducing A_{can}. The balance between increased diffuse radiation and reduced total solar radiation determines whether or not clouds and aerosols (hereafter referred to as "cloudiness") enhance A_{can} (Alton, 2008; Mercado et al., 2009).

To add complexity, the DFE is modulated by factors affecting A_{can}, including latitude, canopy architecture, above- and in-canopy microclimate, leaf biophysical and biochemical properties, and soil properties (all referred to as "site characteristics" hereafter). In addition, secondary cloudiness effects such as changes in solar radiation spectrum or indirect changes in air temperature and VPD (through changes in solar radiation) modulate DFE as well. Not surprisingly, observed responses of A_{can} to cloudiness are diverse (for overviews, see Durand et al., 2021; Kanniah

* Corresponding author at: Meteorology and Air Quality Section, Wageningen University, 6708PB Wageningen, the Netherlands.
E-mail address: kevin.vandiepen@wur.nl (K.H.H. van Diepen).
[1] Current address, Research Institute of Agriculture and Life Sciences, Seoul National University, Seoul, Republic of Korea.

https://doi.org/10.1016/j.agrformet.2025.110597
Received 15 November 2024; Received in revised form 6 March 2025; Accepted 28 April 2025
Available online 6 May 2025

et al., 2012): in some cases, cloudiness increased A_{can} compared to clear skies (e.g. Hollinger et al., 1994; Liu et al., 2022), whereas in other cases it did not (e.g. Alton et al., 2007; Kanniah et al., 2013), and this lack of consensus has been repeatedly emphasized (Alton, 2008; Cheng et al., 2015; Durand et al., 2021).

There is an inability to explain why the DFE occurs at some observational sites but not others. This inability is problematic given that the response of vegetation to diffuse radiation is a major source of uncertainty in the land sink of the global carbon budget (Friedlingstein et al., 2023), while the global carbon budget in turn is a major source of uncertainty in climate projections (Arias et al., 2021). We noticed three aspects in the literature that may be responsible for this inability. First, different research groups define and quantify the DFE differently. Hence, even with the same observational dataset, conclusions about the occurrence of DFE may differ between research groups. Second, to our knowledge, no publication has linked cloudiness type to DFE. Different cloudiness types can be expected to alter direct and diffuse radiation differently, which would cause variation in DFE occurrence across observational sites. Third, little is known on the mechanism(s) and magnitude by which site characteristics modulate the DFE (Liu et al., 2022). Different observational sites have different site characteristics, which will convert a given change in solar radiation components under cloudiness to A_{can} differently.

Our objectives were to develop guidelines for a consistent and feasible quantification of the DFE, and, to develop a theoretical framework enabling us to quantitatively determine how cloudiness types and site characteristics cause variation in DFE occurrence. For validation, we analysed the occurrence of DFE using an observational dataset and a canopy photosynthesis model. Our research questions (RQs) were: (1) How can the DFE be quantified accurately from simultaneous observations of solar radiation, cloudiness types and A_{can}? (2) How does the trade-off in diffuse and total radiation, and the DFE, vary across cloudiness types? (3) How does the DFE vary with site characteristics?

2. DFE guidelines and framework

We first reflect on how the literature currently defines and quantifies the DFE. Then, we develop guidelines for quantifying the DFE in a consistent and feasible manner (RQ1). Thereafter, we develop a theoretical framework to qualitatively assess how the DFE varies with cloudiness and site types (RQ2 and RQ3).

2.1. Guidelines for quantifying the DFE

2.1.1. Definition and quantification of the DFE in the literature

There is inconsistency in the use of the term "diffuse fertilization effect". Many papers (e.g. Kanniah et al., 2012; Mercado et al., 2009; Rap et al., 2018) define DFE as a situation where A_{can} increases under cloudy skies, compared to clear skies. For now we refer to this definition as DFE_{GPP}, given that gross primary productivity (GPP; mol(CO_2) m^{-2} s^{-1}) typically represents A_{can} in the carbon cycle research community (Chapin et al., 2006; Wohlfahrt and Gu, 2015). Other papers use DFE when diffuse radiation is used more efficiently by a canopy compared to an equal amount of direct radiation (Alton et al., 2007; Chakraborty et al., 2022; Shao et al., 2020; Wang et al., 2018; Zhou et al., 2021a). In other words, diffuse radiation has a "fertilizing" effect to the canopy's light-use efficiency (LUE; mol(CO_2) mol^{-1}(photon)), and we term this as DFE_{LUE} for now. In addition, in some cases it is unclear which of the two definitions was meant (Gui et al., 2021; Kalidindi et al., 2014; Proctor et al., 2018; Rap et al., 2018; Strada et al., 2015). At last, several papers introduce terms that are phrased slightly differently than DFE, but may still refer to DFE_{GPP} or DFE_{LUE}, or have a different meaning altogether. Examples are the "diffuse radiation effect" (Knohl and Baldocchi, 2008), "diffuse light effect" (Cheng et al., 2015) and "diffuse fertilization efficiency" (Zhou et al., 2021b).

Typical figures on the DFE are (Fig. 1): (a) A_{can} vs. above-canopy ratio of diffuse to total solar radiation (diffuse fraction, f_{dif}), (b) canopy LUE vs. f_{dif}, and (c) A_{can} vs. above-canopy total solar radiation, hereafter referred to as a canopy light response curve (LRC)(Gu et al., 2002), with the data divided into groups of similar f_{dif}. In these figures, A_{can} is generally represented by GPP or occasionally by net ecosystem exchange (NEE; mol(CO_2) m^{-2} s^{-1})(e.g. Alton, 2008; Park et al., 2018; Zhang et al., 2011): the observed quantity from which GPP is estimated. Solar radiation components are often given in the photosynthetically active radiation (PAR) wavelength range (400–700 nm). f_{dif} is the common indicator for cloudiness (Kanniah et al., 2013), but is often not measured together with NEE (Zhou et al., 2021b). Hence, f_{dif} is often estimated or other proxies for cloudiness are used, such as the clearness index (e.g. Gu et al., 2002; Kanniah et al., 2013) or the relative irradiance (e.g. Cirino et al., 2014; Oliveira et al., 2007). Data are recorded at the canopy scale, have a temporal resolution of 10–60 min, and typically cover entire days and growing seasons.

These figures suggest that: GPP has an optimum response to f_{dif}, with a maximum at intermediate f_{dif} (Fig. 1a), canopy LUE increases with f_{dif} approximately linearly and reaches a maximum at $f_{dif} = 1$ (Fig. 1b), and for a given PAR, a larger f_{dif} generally causes a larger GPP (Fig. 1c). Despite this valuable information, a quantification of DFE_{GPP} or DFE_{LUE}

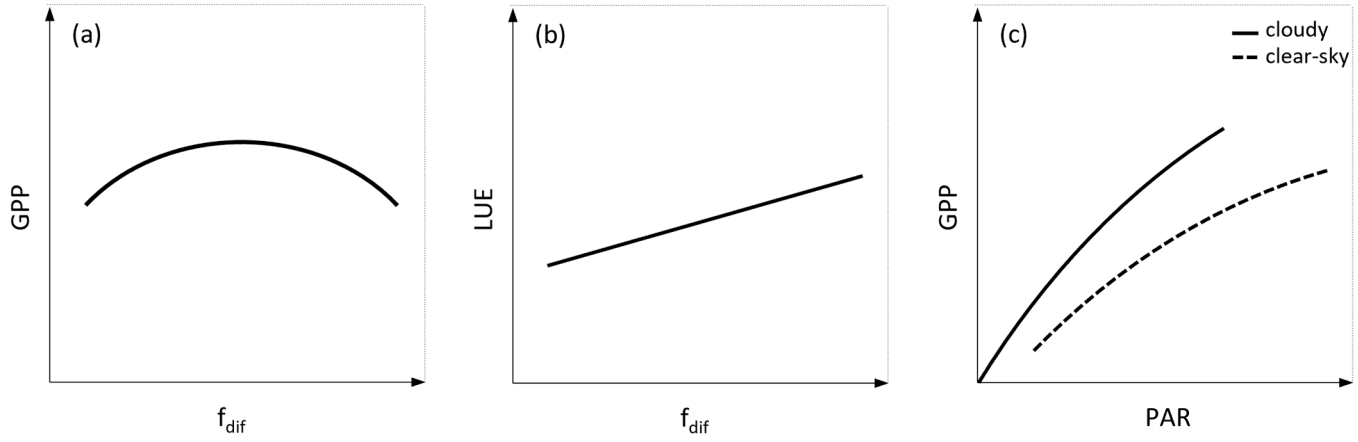

Fig. 1. Schematic overview of commonly used DFE visualizations: GPP vs. f_{dif} (a), canopy LUE vs. f_{dif} (b), and GPP vs. PAR, grouped by different f_{dif} under cloudy and clear-sky conditions (c). See Table S1 for publications using these figures. Abbreviations: GPP, gross primary productivity; LUE, canopy light use efficiency; PAR, photosynthetically active radiation; and f_{dif}, diffuse fraction of PAR.

is impossible or is generally done inaccurately. For instance, DFE_{LUE} cannot be quantified from Fig. 1a, as PAR is not given, preventing the comparison of GPP at equal amounts of direct and diffuse PAR. Using Fig. 1b, neither DFE_{GPP} nor DFE_{LUE} can be quantified since neither GPP nor PAR are given. Fig. 1a does allow to demonstrate DFE_{GPP}, yet we argue that an accurate quantification of DFE_{GPP} is impossible from Fig. 1a– as often shown in the literature – since the impact of cloudiness on GPP is not isolated. Figures such as depicted in Fig. 1 are often constructed from entire days to growing seasons. Hence, any pair of GPP data that differs in f_{dif} will likely differ in time of day or day of year. A difference in GPP is then not solely caused by cloudiness, but also by site characteristics that vary over time. Some authors limited their study period to remove temporal variability in a certain site characteristic (Alton, 2008; Gu et al., 1999; Hemes et al., 2020; Knohl and Baldocchi, 2008; Oliphant et al., 2011; Still et al., 2009; Williams et al., 2016; Zhang et al., 2024), but these are exceptions given the total number of observation-based DFE studies using such figures ($n = 68$; Table S1).

These figures have at least one of two shortcomings: a) there is no connection to existing definitions of the DFE, (b) the response of GPP to just cloudiness is not isolated. In addition to these shortcomings, no one DFE quantification protocol is used consistently by the community. To our knowledge, only Gu et al. (1999) discuss and provide a complete protocol to quantify the DFE systematically. Yet, their protocol has been applied infrequently, and if so, partially (Appendix A). The use of different protocols causes random variation in the sign and magnitude of derived DFE. We are thus in need of a systematic, feasible protocol that encourages to quantify the DFE accurately. In the next subsection we propose two guidelines that should underly any protocol to quantify the DFE. In addition, we discuss the consequences of those guidelines for the major steps in such protocol.

2.1.2. *New guidelines for quantifying the DFE*

Our two guiding principles for the quantification of the DFE are:

a) The DFE is an *effect*, hence two situations need to be compared to know its sign and magnitude.
b) Those two situations should differ only in the factor that *causes* the effect. For DFE_{GPP}, that factor is the presence of cloudiness and for DFE_{LUE} it is the fraction of diffuse radiation.

Guideline a) implies that a baseline needs to be defined against which the observation of interest can be compared. For DFE_{GPP}, the baseline should be a situation without cloudiness (i.e. clear-sky). For DFE_{LUE}, any two situations that differ in f_{dif} can be compared. However, for consistency with DFE_{GPP}, we suggest to quantify DFE_{LUE} relative to a clear-sky baseline as well. In the operationalisation of guideline a), one must ensure that the identification of a clear-sky situation does not depend on anything else than the presence of cloudiness. In practice, threshold values for f_{dif} or a clearness index are often used (Appendix A). On clear-sky days, both proxies change diurnally and the threshold used to determine the clear-sky baseline should account for this variation.

Guideline b) is a ceteris paribus assumption ('all else being equal'), which in observational field studies is unattainable. A setup that would come close would be an observational study over a single surface type, at two locations that are sufficiently close to have identical site characteristics, yet sufficiently separate to be exposed to either clear-sky or cloudy conditions. Such data are rare, so in practise time series from a single location are used. In that case, the two situations required to determine the effect (guideline a) will always be displaced in time, and as a consequence, more than just the causal factor differs. Thus, in the operationalisation of guideline b), one can only minimize (not eliminate) temporal variation in factors other than the causal factor. The two time scales that dominate temporal variations in photosynthesis are the diurnal and seasonal cycles, whereas on top of that there will be day-to-day variation in weather conditions. This results in two options: (1) using two moments directly following one another on the same day, or (2) using moments at the same time of day on consecutive days. Both options remove the seasonal variation of site characteristics. Option 1 minimizes day-to-day variability of site characteristics, but allows some diurnal variability, while option 2 does the reverse. When quantifying DFE_{LUE} an additional issue arises: under a ceteris paribus assumption, GPP at two f_{dif} levels requires equivalent PAR and time of day. In practice, this is rarely possible, as a given PAR is typically reached on a time of day that differs between clear-sky and cloudy days (Gu et al. 1999). Therefore when quantifying DFE_{LUE}, diurnal variability in site characteristics can be minimized only to some extent.

2.2. *Framework to clarify DFE variation*

Next, we use a version of Fig. 1c (Fig. 2) to illustrate how the sign and magnitude of DFE_{GPP} and DFE_{LUE} depend on cloudiness and site characteristics.

The starting point is the GPP of a clear-sky moment (A). To arrive at the GPP of a corresponding cloudy moment, changes in f_{dif} and PAR need to be accounted for: increasing f_{dif} causes a vertical increase from the clear-sky canopy LRC towards the overcast canopy LRC (i.e. f_{dif} close to 1, D) to an intermediate point (B), while the change in PAR leads to a step along the cloudy canopy LRC to either C1, C2 or C3. The difference in GPP between A and B represents DFE_{LUE}, that between A and C1-C3 represents DFE_{GPP}. DFE_{LUE} is generally positive, as cloudy canopy LRCs usually are located above clear-sky ones (although see Zhou et al., 2021b). DFE_{GPP} is positive if C is above A (e.g. C2 and C3). The cloudy moment represented by C1 causes negative DFE_{GPP}, as the reduction in GPP due to smaller PAR is larger than the increase in GPP due to larger f_{dif}. The cloudy moment represented by C3 caused both PAR and f_{dif} to increase, which represents a situation with cloud enhancement (CE; Appendix A), resulting in a large increase in GPP.

Several aspects are evident from Fig. 2: (i) DFE_{LUE} (ΔGPP) depends both on site characteristics (the vertical shift of the LRC for a given change in f_{dif}, or ΔGPP Δf_{dif}^{-1}) and on cloudiness (Δf_{dif}), and overall varies with PAR, (ii) DFE_{GPP} (ΔGPP) depends on DFE_{LUE}, site

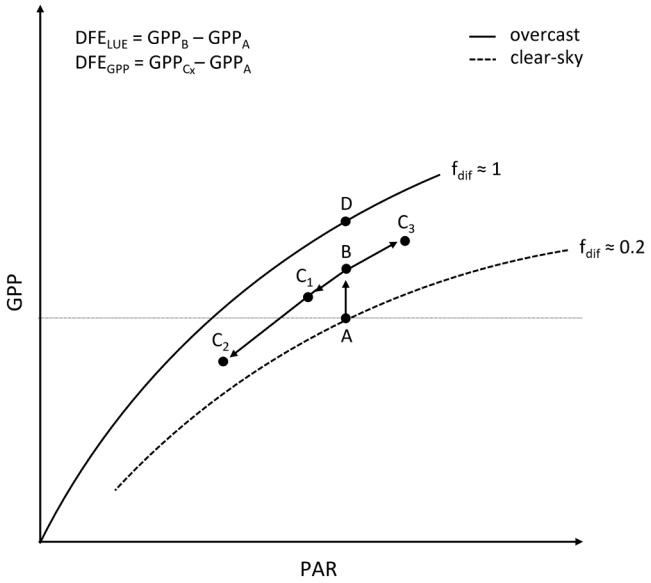

Fig. 2. Schematic of canopy light response curves illustrating DFE_{LUE} and DFE_{GPP} (adapted from Fig. 1c). Clear-sky GPP (A) is compared to cloudy GPPs (C1-C3). D indicates the GPP when f_{dif} is largest (i.e. $f_{dif} = 1$), which is typical for overcast conditions. The horizontal line indicates when DFE_{GPP} switches sign. Note that clear-sky f_{dif} is not zero due to atmospheric molecular scattering. Abbreviations: GPP, gross primary productivity; PAR, photosynthetically active radiation (top of canopy); f_{dif}, diffuse fraction of PAR; DFE_{GPP}, diffuse fertilization effect on GPP; and DFE_{LUE}, diffuse fertilization effect on canopy light use efficiency.

characteristics ($\Delta GPP\ \Delta PAR^{-1}$) and cloudiness ($\Delta PAR$), (iii) the larger DFE_{LUE} is, the larger the chance that DFE_{GPP} is positive, (iv) cloudiness types that strongly increase f_{dif} and minimally reduce PAR very likely cause positive DFE_{GPP} (large jump from A to B and minimal shift from B towards C1), (v) site characteristics that strongly increase canopy LUE with increasing f_{dif} cause large DFE_{LUE} and likely cause positive DFE_{GPP} (large jump from A to B), (vi) CE very likely causes positive DFE_{GPP}, as both f_{dif} and PAR increase (jump from A to B and shift from B to C3).

DFE_{LUE} and DFE_{GPP} appear to represent different aspects of cloudiness effects on A_{can}. Also, there is a causal relation between the two: the magnitude of DFE_{LUE} influences the sign and magnitude of DFE_{GPP}. In other words, DFE_{LUE} indicates a *potential* increase in GPP under cloudiness, if PAR would not change, that can be converted to *actual* GPP increase (DFE_{GPP}) after accounting for the change in PAR. To make this relation explicit, hereafter we refer to DFE_{LUE} and DFE_{GPP} as **potential** DFE (PDFE) and **actual** DFE (ADFE), respectively.

To understand how ADFE varies with cloudiness types and site characteristics, we need to know (i) how changes in f_{dif} and PAR vary with cloudiness types, and (ii) how site characteristics affect canopy LRCs. Regarding (i), it is sufficient to *know* (i.e. observe) how changes in f_{dif} and PAR vary across cloudiness types to study the DFE. To *understand* why f_{dif} and PAR vary across cloudiness types requires detailed information about cloud composition, thickness and structure, which is beyond the scope of this paper. For (ii), we need to identify site characteristics that affect canopy LRCs and the mechanisms by which they do so. The position of canopy LRCs in Fig. 2 reflects how efficient the canopy converts PAR into GPP. That conversion takes place in three steps: (i) the interception of PAR photons by the canopy, (ii) the distribution of those PAR photons over the canopy leaf area, yielding PAR intensities at leaf surfaces, and (iii) the LUE of leaves at those respective PAR intensities, yielding leaf photosynthesis (and A_{can}, expressed by GPP, as the sum of all leaf photosynthesis). Site characteristics that maximize canopy interception of PAR and optimize the distribution of PAR inside the canopy with local leaf LUE, under cloudiness, will maximize the PDFE and the chance of causing ADFE. In Table S2 we provide an overview of site characteristics that have been suggested to affect the PDFE. We indicated per site characteristic the mechanism (i, ii or iii) by which it affects PDFE and the typical time scale by which it varies.

3. Materials and methods

To illustrate our guidelines and validate our framework, we conducted analyses using an observational dataset and a canopy photosynthesis model. The observation-based analysis served to quantify ADFE across cloudiness type (RQ2), whereas the model-based analyses served to quantify PDFE across site characteristics (RQ3). In both analyses we applied our proposed guidelines and used our framework to link PDFE to ADFE.

3.1. Observations

3.1.1. Site description and instrumentation

In the spring of 2018, a field campaign was conducted at the Terrestrial Environmental Observatory Selhausen, which is located in the lower Rhine embayment in western Germany (50°52′09'' N, 6°27′01'' E, 104.5 m altitude) in a region dominated by agriculture. The site is equipped with micrometeorological instrumentation in accordance with ICOS class 1 standards. The field campaign provided supplementary instrumentation to the site, which yielded a comprehensive observational dataset of soil, plant and atmospheric quantities for a test field on which winter wheat (*Triticum aestivum* L.; variety Premio) was sown in October 2017 (see Vilà-Guerau De Arellano et al., 2020). Here we summarize the aspects relevant to our analysis.

The campaign lasted from the beginning of May until the end of June, covering most developmental stages (booting to ripening; Zadoks scale 4.3 – 9.1) of winter wheat. The test field covered 9.8 ha and was surrounded by other croplands. The soil was classified as Orthic Luvisol with a silt loam texture consisting of 20 % clay, 67 % silt and 13 % sand. Data presented here was recorded using an eddy covariance (EC) system (SN1185 Irgason EC150, Campbell Scientific, Inc., Logan, Utah, USA; PTB101B pressure sensor, Vaisala Inc., Helsinki, Finland) located in the centre of the test field at 1.93 m above the ground, four PAR sensors (three LI-190R, Li-Cor Inc. Biosciences, Lincoln, Nebraska, USA; one BF5, Delta-T Devices, Cambridge, UK), of which one Li-190R faced the canopy and the BF5 sensor measured diffuse PAR, a pyranometer (CNR4, Kipp & Zonen B.V., Delft, Netherlands) yielding global radiation above the canopy ($S^{\downarrow}$), a ceptometer (SunScan, Delta-T Devices, Cambridge, UK), and two cameras of which one faced the sky and the other the field.

3.1.2. Analysis strategy

For quantifying PDFE and ADFE, we limited our observational analysis to a two-week period (May 7–20), to limit seasonal variability in site characteristics while maintaining sufficient sample size for various sky conditions. The chosen study period was selected as it included (i) a sufficient sample size for the sky conditions necessary to quantify the PDFE and ADFE (per cloudiness type), (ii) a soil water content close to field capacity (based on soil texture and the classification scheme of Saxton and Rawls (2006)), minimizing plant drought stress, and (iii) a developmental stage of wheat (booting stage) with high photosynthetic capacity, thus minimizing the signal-to-noise ratio in NEE. Leaf area index (LAI) increased from 4.6 to 5.5 $m^2\ m^{-2}$ during this period and remained stable afterwards. The observed increase in LAI may have been caused primarily by the way the ceptometer determines LAI: elongated stems and head emergence during the study period may have been falsely detected by the ceptometer as leaf area. Canopy height throughout the study period was approximately 0.5 m. A summary of micrometeorological conditions relevant to GPP is shown in Fig. S1.

3.1.3. Data processing

We represent A_{can} by GPP, which we derived following Tramontana et al. (2020):

$$GPP = -NEE + R_{eco} \quad (1)$$

where R_{eco} is the ecosystem respiration. *NEE* was obtained from EC and fluxes were processed with the LiCor EddyPro v6.2.2 software to obtain 10-min averages. The relatively short averaging period was necessary to capture GPP responses to variable weather conditions. Using 10-min average fluxes (rather than the conventional 30-min averages) was justified by the fact that measurements were done relatively close to the surface, so that the covariance between vertical wind speed and CO_2 concentration at timescales beyond 10 min was small (e.g. Feng et al., 2017). R_{eco} was predicted from nighttime *NEE* and air temperature following Reichstein et al. (2005). The temperature sensitivity parameter E_0 was separately fitted using a linear regression protocol (MATLAB 2020b, MathWorks Inc.). Air temperature, rather than soil temperature, was used in predicting R_{eco}, as we found a higher correlation of the former with nighttime *NEE* (see Lasslop et al., 2012). We filtered data ($n = 269$) for nighttime ($S^{\downarrow} < 20\ W\ m^{-2}$)(Lasslop et al., 2009), high quality flags following Foken et al. (2004), and absence of precipitation.

PAR was represented as the average of PAR measured by two LI-190R sensors. We subtracted observed canopy reflected PAR to remove potential variation in PAR between clear-sky and cloudy moments. f_{dif} was calculated as the ratio of diffuse PAR to PAR as measured by the BF5 sensor and a third Li-190R sensor. PAR components were recorded at 1 Hz, but processed to 10-minute averages to match the temporal resolution of GPP.

3.1.4. Data analysis

In accordance with our proposed guidelines (Section 2.1.2), we

quantified the ADFE by comparing moments of GPP at equal time of day ($ADFE_t$), and defined a clear-sky reference GPP that accounted for diurnal variation in f_{dif}. Additionally to $ADFE_t$, we quantified ADFE by comparing daily sums of GPP ($ADFE_{day}$). $ADFE_t$ follows option 2 in Section 2.1.2, and $ADFE_{day}$ is an adapted version of option 1.

Clear-sky reference GPP for $ADFE_t$ and $ADFE_{day}$ were obtained as follows. We started by creating a clear-sky reference f_{dif} (f_{dif_cs}), by grouping f_{dif} by time of day. Per group, we selected the minimum value. GPP moments at $f_{dif} < f_{dif\_cs} + 0.1$ were labelled as clear-sky. The limit of 0.1 was an arbitrary choice. We constructed a smooth composite diurnal cycle from clear-sky GPP groups using first a moving 30-min median window. Data was further smoothed with a 30-min moving average window to reduce statistical noise in GPP that stemmed from NEE, which is an artifact of the EC method. Smoothed GPP medians were time-integrated across daytime ($\beta > 10°$) to obtain a clear-sky reference GPP sum ($GPP_{ref,day}$). These steps were repeated to obtain clear-sky PAR and GPP interquartile range (IQR). Characteristics of our clear-sky reference diurnal cycle are shown in Fig. 3.

$ADFE_t$ was calculated as the difference between the 75th percentile of a clear-sky GPP group and the GPP of cloudy moment ($f_{dif} > f_{dif\_cs} + 0.1$). $ADFE_{day}$ was calculated as the difference between $GPP_{ref,day}$ and the daily GPP sum of a given day. Daytime data were filtered ($n = 945$) for high quality flags following Foken et al. (2004) and absence of precipitation. Data filtering caused gaps in the GPP time series, of which some were filled based on an estimated LUE (linear fit with f_{dif}) in combination with observed PAR.

We tested the hypothesis that $ADFE_t$ occurs often under cloudiness types that cause large f_{dif} at small PAR reductions, in two steps. First, we determined f_{dif} and PAR for ten cloudiness types (nine cloud types and an aerosol class, Table S3) and compared these to combinations of f_{dif} and PAR under all cloudy moments that corresponded to a GPP equivalent with clear-sky GPP (shaded area Fig. 3c). Second, we determine $ADFE_t$ frequency per cloudiness type by temporally overlaying satellite images with GPP. Due to their difference in temporal resolution and phase, elements of both time series were artificially repeated to obtain 1-second resolution. Some operational aspects of these two steps are described below.

A change in atmospheric transmissivity (τ_{atm}) was used to characterize the effect of the atmosphere on PAR, independent of time-of-day, date or latitude. f_{dif} already represents that effect, since there is no diffuse radiation at the top of the atmosphere. We calculated τ_{atm} as the ratio of $S^{\downarrow}$ to its value at the top of the atmosphere ($S^{\downarrow}_{TOA}$). $S^{\downarrow}_{TOA}$ was estimated according to Moene and Van Dam (2014). Cloud types were derived from satellite images following Mol et al. (2023a) at a 15-min resolution, and at a 5 km radius (i.e. four satellite pixels) around the site. Their algorithm creates combinations of satellite-observed cloud

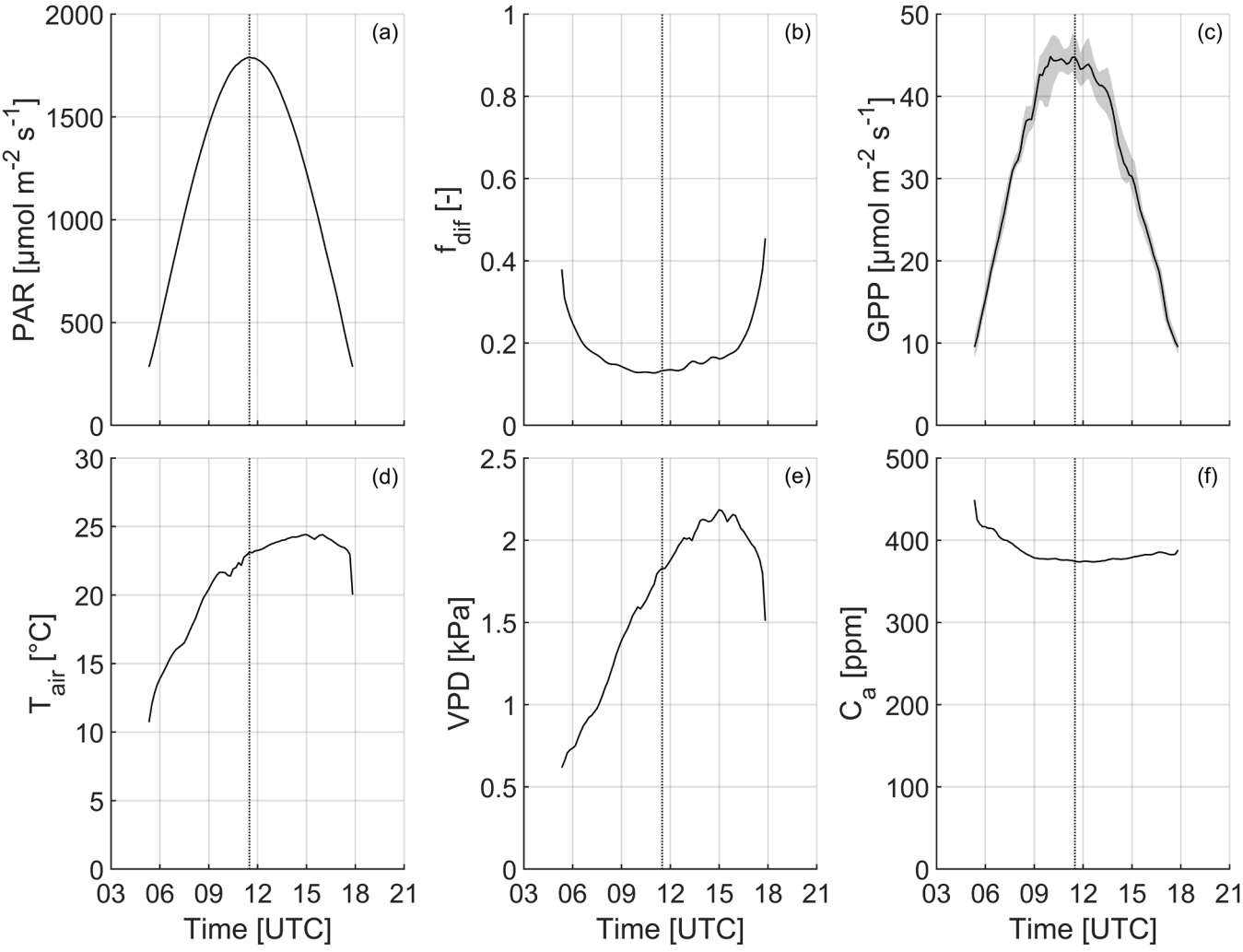

Fig. 3. Clear-sky reference diurnal courses of PAR (a), f_{dif} (b), GPP (c), air temperature (T_{air}; d), vapor pressure deficit (VPD; e), and ambient CO_2 concentration (C_a; f) based on observed clear-sky conditions ($f_{dif} < f_{dif\_cs} + 0.1$) within the study period. The vertical dotted bar indicates solar noon. The shaded area in panel c indicates the interquartile range of clear-sky GPP. Clear-sky reference T_{air}, VPD and C_a were not used in the observational analysis, but were used together with PAR and f_{dif} as input for the canopy photosynthesis model (Section 3.2).

top pressure (CTP) and cloud optical thickness (COT) to which cloud types are assigned using cloud type definitions of the International Satellite Cloud Climatology Project (Table S3). Limitations of the algorithm are: (i) the spatial resolution of the satellite pixels (Mol et al., 2023a), (ii) the quality of the calibration of imagery sensors (these calibrations are regularly tested, but on monthly averaged data, not hourly), (iii) the inability to distinguish multiple cloud types in case of a multi-layer cloud system (Mol et al., 2023b), and (iv) the assumption that a given cloud type only occurs within the defined range of CTP and COT. A notable consequence of (i) is that the COT of a patchy cloud field, such as occurs with Cumulus and Altocumulus, will be lower (i.e. optically thin) than the COT of individual clouds as the former is a result of the combination of individual clouds and the clear-sky gaps in between. Moments in the study period that were neither clear-sky ($f_{dif\_cs} + 0.1$) nor assigned to a cloud type were pooled together into a single class which we labelled "aerosol". To realise this, we adapted the "irradiance weather classification" procedure in Mol et al. (2023a): (i) their clear-sky class definition was expanded with the restriction that $f_{dif} \leq f_{dif\_cs} + 0.1$, and (ii) a new class named "aerosol" was introduced that was defined similar to the clear-sky class, but with the restriction that $f_{dif} > f_{dif\_cs} + 0.1$. To prevent moments of undetected clouds to enter the aerosol class, we added a restriction to the variability of $S^{\downarrow}$ (Table S3). We labelled this weather class as "aerosol", as the atmospheric disturbance behind the increased f_{dif} likely involved excessive aerosol loads or indirect aerosol effects such as hygroscopic growth (Gristey et al., 2022; Mol et al., 2024). Typical (non-excessive) variation in aerosol load caused predicted f_{dif} to vary between 0.1 and 0.2 at four high-latitude sites within a few hours of solar noon (Ezhova et al., 2018), which in our analysis would be captured in the clear-sky class. The aerosol class included moments that were characterized by f_{dif}-values in the range of 0.22–0.55 (time-of-day dependent) and low variability in $S^{\downarrow}$ even relative to clouds such as Cirrus.

Per cloudiness type, we explored how often CE caused $ADFE_t$. We defined CE following Mol et al. (2023a)(Table S3), but with a modification since several long-lasting (> 30 min) CE events were detected within our aerosol class. These CE events were weak in amplitude, but persistent over time. To restrict CE events to primarily clouds, we made the description of CE stricter (see Table S3). The description of the variable weather class, in turn, was loosened up as (cloud-induced) CE would occur less frequently in our dataset. Fig. 4 shows examples of cloud and irradiance classifications.

To quantify the PDFE from observations, we constructed canopy LRCs from GPP, PAR and f_{dif}. GPP was first divided into bins of PAR with a range of 200 μmol m^{-2} s^{-1}. Within a given PAR-bin, GPP was divided based on f_{dif}: clear-sky ($f_{dif} < f_{dif\_cs} + 0.1$), cloudy ($f_{dif} > f_{dif\_cs} + 0.1$ and $f_{dif} < f_{dif\_cs} + 0.7$) and overcast ($f_{dif} > f_{dif\_cs} + 0.7$). The limit of 0.7 was chosen such that f_{dif} would not need to be exactly 1 in order to be classified as overcast.

3.2. Model

3.2.1. Model description

To quantify the influence of site characteristics on the PDFE, we used a one-dimensional (1D) multilayer steady-state A_{can} model consisting of two sub-models: a coupled leaf photosynthesis (A)-stomatal conductance (g_s) model and a radiative transfer (RT) model.

Leaf-level coupled A-g_s model. A and g_s were represented by the models of Farquhar et al. (1980) and Leuning (1995) respectively. Both models are extensively described elsewhere (Damour et al., 2010; Von Caemmerer, 2013), so we do not provide a full description here. The g_s-model of Leuning (1995) was chosen, as it accounts for effects of A and air vapor pressure deficit (VPD). We used Arrhenius temperature response functions to describe temperature dependence of A (Silva-Perez et al., 2017). The model did not explicitly account for leaf boundary layer or mesophyll resistance, so that CO_2 diffusion into the leaf was assumed to depend on stomatal resistance only and A was simulated based on the

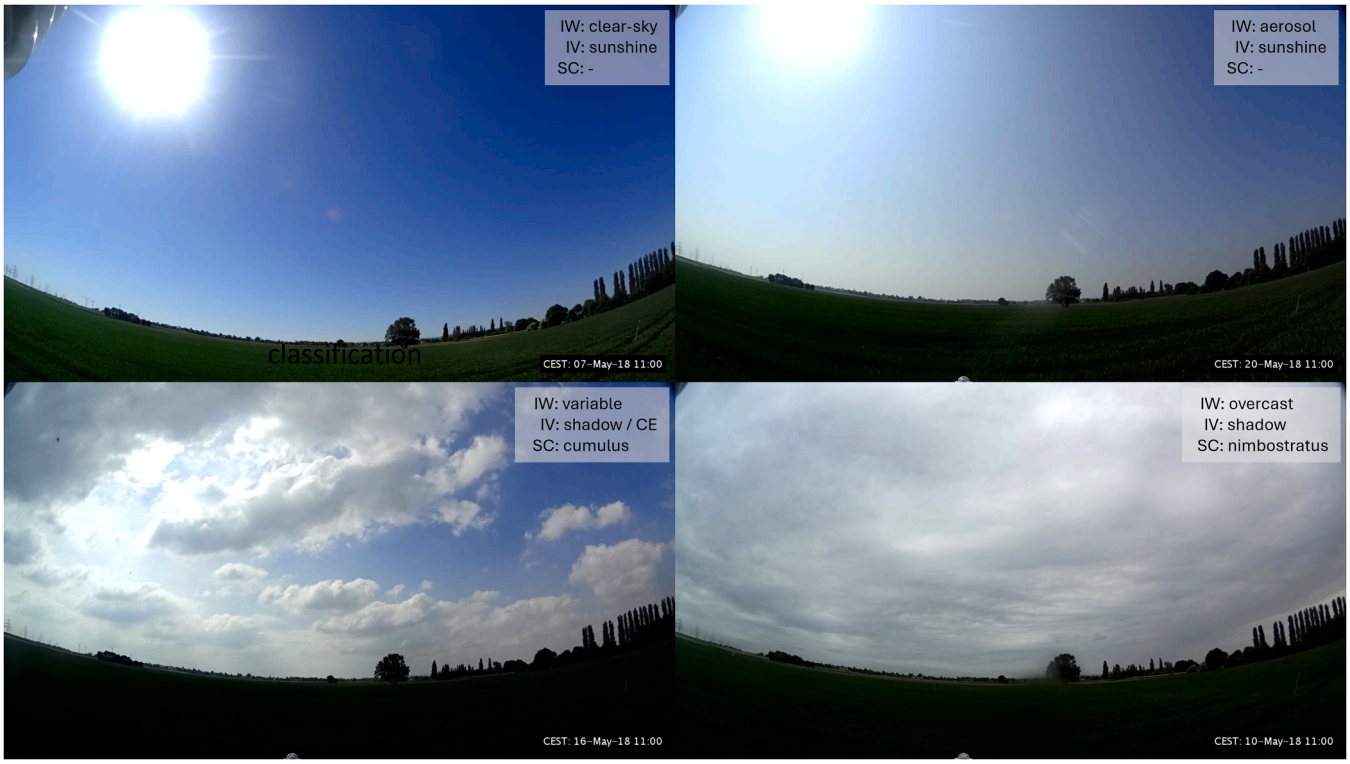

Fig. 4. Camera snapshots at 11:00 CEST on various days within the study period. Text indicates the irradiance and cloud conditions based on the classifications of Mol et al. (2023a)(Table S3). Note that the camera's inclination changed slightly after May 7, causing the view angle to be oriented closer to the surface in May 10, 16 and 20. Abbreviations: IV, irradiance variability classification; IW, irradiance weather type classification; SC, satellite cloud type classification.

CO_2 concentration of the leaf intercellular airspace (C_i). Leaf boundary layer was not considered, since leaves in the field are generally well coupled to the atmosphere (Niinemets et al., 2009). Mesophyll resistance was implicitly accounted, as photosynthetic parameter values were estimated from observations based on C_i, largely compensating for prediction errors in A due to a lack of mesophyll resistance (Knauer et al., 2020). Maximum carboxylation rate and maximum electron transport rate decreased with cumulative leaf area to mimic the vertical gradient of leaf nitrogen content in natural canopies (Walker et al., 2014), a common approach in land-surface models (Bonan et al., 2011; Clark et al., 2011; Krinner et al., 2005). We used a wheat-specific gradient in leaf nitrogen content based on Hikosaka et al. (2016). For more details, see Appendices B and C.

Canopy RT model. Canopy RT was represented by a 1D model containing elements from Goudriaan (1977), Goudriaan and Van Laar (2012) and Goudriaan (2016)(detailed description in Appendices D and E). The model follows the turbid medium approach, where a canopy is treated as a green gas with leaves represented as infinitely small elements that absorb and scatter PAR and are distributed randomly in horizontal layers (Disney, 2016; Qin and Liang, 2000; Ross, 2012). We divided the canopy into 10 horizontal layers of equal leaf area, which is a typical number in land surface models (e.g. Clark et al., 2011). Leaves were assumed to scatter PAR once, allowing to describe canopy extinction of PAR with Lambert-Beer's exponential law (Disney, 2016). Orientation of sunlit leaves was described following Campbell and Norman (1989), with 100 equally spaced orientations. Diffuse PAR was assumed to be anisotropic, arriving from 9 sky zones in varying intensity following a standard overcast sky (Goudriaan, 1977; Grace, 1971). Each diffuse PAR stream had a specific canopy extinction rate. We assumed that adaxial and abaxial sides of leaves did not differ in their physiology, so that total diffuse PAR was equal for all leaves in a given layer, regardless of their orientation (Campbell and Norman, 2000). We used separate reflection coefficients for soil and canopy, instead of the effective soil-canopy reflection coefficient used by Goudriaan (1977), to maintain a flexible model structure. Model calculations were based on the middle points of leaf layers, sunlit leaf angle segments and sky zones, which introduced a minor (<1 %) discretization error in predicted GPP and the canopy PAR budget.

Canopy photosynthesis model. The RT model predicted absorbed PAR for all leaf surfaces in the canopy. The A-g_s model used absorbed PAR, leaf temperature, VPD, CO_2 and O_2 concentrations as input and predicted the leaf apparent photosynthetic rate (mol(CO_2) m^{-2}(leaf) s^{-1}). The sum of predicted apparent A, scaled by respective leaf areas (m^2(leaf) m^{-2}(ground)), yielded GPP (Wohlfahrt and Gu, 2015). Predicted GPP was an approximation of true GPP, since the model ignored apparent photosynthesis of other above-ground wheat organs (e.g. stems and ears).

Leaf temperature, CO_2 concentration and VPD were set equal to above-canopy air temperature, CO_2 concentration and VPD at 1.93 m height, respectively, as observed by the EC system (Fig. 3d–F). In-canopy observations of these quantities were too sparsely available. O_2 concentration was set to 0.21 mol mol^{-1}. Above-canopy PAR components were represented similarly as in the observational analysis. β was predicted according to Moene and Van Dam (2014).

3.2.2. Model optimization

The A_{can} model was optimized against observed GPP to test the PDFE sensitivity of winter wheat during the study period. Optimized parameters ($n = 5$) were all part of the coupled A-g_s model: maximum electron transport rate normalised at 25 °C (J_{max25}), activation energy of J_{max25}, quantum yield to electron transport, slope of stomatal sensitivity to net photosynthesis, and stomatal sensitivity to VPD (Table C1). Optimized values corresponded to lowest root mean square errors and were comparable to published values (Appendix F).

After optimization, observed and modelled GPP matched well ($r^2 = 0.9$; Fig. S2). We consider the model's performance, in terms of r^2 and slope, acceptable for starting points (clear skies) and endpoints (cloudiness) of the PDFE.

3.2.3. Model analysis

Predicted PDFE per time of day ($PDFE_{mod\_t}$) was determined as the ratio between simulated clear-sky GPP and a GPP under identical clear-sky conditions (including PAR) except that f_{dif} was increased by 0.7 (referred to as "perturbed clear-sky"). We focussed on GPP ratio, and not absolute GPP difference, since the latter strongly scales with PAR. The increase of 0.7 was chosen so that clear-sky moments ($f_{dif} < f_{dif\_cs} + 0.1$; Fig. 3b) at all times of day would experience the same perturbation. Since only f_{dif} differed between the two predictions, $PDFE_{mod\_t}$ aligned with the definition of PDFE. We increased f_{dif} by a large margin to maximize $PDFE_{mod\_t}$. The clear-sky day was represented in the model by observed clear-sky reference conditions (Fig. 3).

We simulated how $PDFE_{mod\_t}$ would change per site characteristic (hereafter referred to as "model scenario") during a clear-sky day. Model scenarios (Appendix G) were chosen such as to capture the natural range of values across observational sites. Site characteristics included LAI, latitude, leaf inclination angle distribution (LIAD), canopy nitrogen distribution, leaf reflectance, and leaf transmittance. LAI, LIAD, leaf reflectance and transmittance were chosen to facilitate comparison with Knohl and Baldocchi (2008), which to our knowledge is the only study to quantify PDFE for multiple site characteristics and over a large range of values. Latitude was chosen due to importance of β to PDFE (Gu et al., 1999). Canopy nitrogen distribution, albeit having previously received little attention, was included as it affects the distribution of photosynthetic capacity in the canopy.

4. Results

In this section we report on the observation-based and model-based analyses. Section 4.1 illustrates how the application of our guidelines results in a quantification of ADFE and PDFE (RQ1). Section 4.2 quantifies the ADFE across cloudiness types (RQ2). Section 4.3 quantifies the PDFE across site characteristics (RQ3).

4.1. Quantification of the DFE

Within the study period, two days with clouds showed a substantial increase in daily GPP (19 and 10 % on May 11 and 12), compared to clear-sky reference GPP (Fig. 5), thus an $ADFE_{day}$ occurred on these days. These two days were characterized by a 20 % reduction in PAR and a 0.41 increase in f_{dif} relative to the reference day. Days with predominantly overcast conditions (May 10, 14 and 16) showed substantially reduced GPP. In these cases, nearly all PAR was diffuse (Fig. 5b), but the concomitant reduction in PAR was too extensive to result in an increased GPP. Some days showed similar solar radiation characteristics as May 11 and 12 (e.g. May 18 and 19), but did not show an increase in GPP. Other days that showed noticeable increases in diffuse PAR and minor reductions in total PAR (i.e. May 9, 17 and 20) also did not show increased GPP. We discuss this inconsistent pattern between solar radiation characteristics and daily GPP sums elsewhere (Appendix H).

Despite daily GPP being higher than $GPP_{ref,day}$ on only two days, other days did contain moments (10-minute intervals) with $ADFE_t$ (Fig. 6), and the two days with higher daily GPP contained moments at which GPP was beneath clear-sky GPP. On some days, daily GPP could have surpassed $GPP_{ref,day}$ (e.g. May 20; Fig. 6d), but this was thwarted due to large drops in PAR under clouds (Fig. 6h). Periods with CE often led to $ADFE_t$ (see also Section 4.2), but the additional GPP could often not compensate for the dramatic loss in GPP under concomitant cloud shadows, such as on May 16 (Fig. 6 g). Clear-sky GPP sum before solar noon was 9 % higher than that after solar noon (Fig. 3c), but this did not

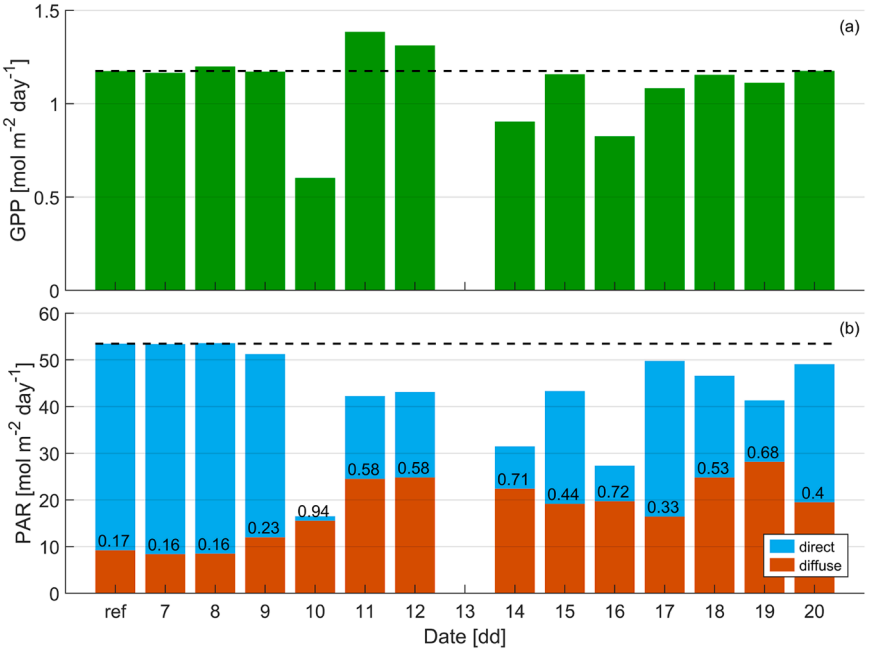

Fig. 5. Daily sums of GPP (a), direct PAR (b; light blue) and diffuse PAR (b; red). Numbers in (b) indicate the fraction of diffuse PAR (f_{dif}). Dashed horizontal lines indicate GPP (a) and PAR (b), for the reference clear-sky day. Abbreviations: GPP, gross primary productivity; PAR, photosynthetically active radiation (top of canopy).

make it more likely for $ADFE_t$ to occur in the afternoon. In fact, we did not detect any increased likelihood for $ADFE_t$ to occur at any time of day, possibly because the occurrence of cloudiness was not bound to specific times of day (not shown). Overall, $ADFE_t$ occurred during 32 % of all non-clear moments and was characterized by an average 11 % increase in GPP relative to clear-sky GPP, and by a 15 % increase when CE was present for at least half of the time.

Next, we quantified the PDFE. The wheat canopy responded with increased GPP (by 30–45 %) to an increase of f_{dif} across observed PAR (Fig. 7). Thus, any increase of f_{dif} increased canopy LUE. PDFE was largest at intermediate PAR in absolute terms (Fig. 7b), but at low PAR in relative terms (Fig. 7c). The spread in GPP at a given PAR and for a given f_{dif}-bin is the result of statistical noise in NEE, variation in site characteristics such as air temperature and VPD, variation in f_{dif} within a bin, and, in the case of clear-sky conditions, a hysteresis effect of GPP between morning and afternoon. GPP increased with PAR under all weather conditions (Fig. 7a). Only under clear-sky conditions at solar noon, GPP showed a subtle decline, confirming previous observations (e.g. Mercado et al., 2009). We did not observe this decline when using 30-minute averaged fluxes (not shown).

Positive PDFE allowed cloudiness to reduce PAR without reducing GPP below clear-sky GPP (Fig. 8), thus creating $ADFE_t$. Moments of CE (i.e. cloudy PAR > clear-sky PAR) resulted in large $ADFE_t$, as an increase in both PAR and f_{dif} increased GPP (Fig. 7a). Especially PDFE at high clear-sky PAR (Fig. 7b) caused large $ADFE_t$, when PAR under cloudy conditions remained high as well (e.g. Fig. 8b). Fig. 8 illustrates the shared role of cloudiness and site characteristics in causing $ADFE_t$: the positive PDFE, facilitated by site characteristics ($\Delta GPP\ \Delta f_{dif}^{-1}$ at a given PAR) and cloudiness (Δf_{dif}), was necessary to balance loss in GPP due to reduced PAR under cloudiness.

4.2. Cloudiness types and ADFE

We quantified the frequency with which different cloudiness types caused $ADFE_t$. At our site, clouds were detected for 62 % of daytime ($\beta > 10°$) with Cirrus and Altocumulus as the most frequent occurring cloud types (each 19 % of cloud detection time) and Stratus the least frequent (5 %; Table 1). Aerosol conditions occurred 12 % of daytime. After temporally synchronising GPP with irradiance and cloud classifications, several aspects became visible: (i) NEE was inherently noisy over time, so that even on perfectly clear days, GPP was sometimes larger and sometimes smaller than the IQR of clear-sky GPP (Fig. 9a), (ii) predicted clear-sky $S^{\downarrow}$ was nearly identical to observed clear-sky $S^{\downarrow}$ (Fig. 9a), (iii) CE ($S^{\downarrow}$ > modelled clear-sky $S^{\downarrow}$) occurred under most cloud types and exceeded predicted clear-sky $S^{\downarrow}$ up to 40 % (Fig. 9b), (iv) cloudy weather that was neither overcast nor variable was not assigned a weather class (Fig. 9b–d), and, (v) some cases where $S^{\downarrow}$ implied the presence of clouds were not detected by the cloud classification algorithm (Fig. 9d; 12–14 UTC).

We determined f_{dif} and τ_{atm} per cloudiness type (Fig. 10). Aerosol conditions maintained the largest τ_{atm}, followed by optically thin cloud types (Cirrus, Altocumulus, Cumulus), intermediately thick cloud types (Cirrostratus, Altostratus, Stratocumulus) and thick cloud types (Cumulonimbus, Nimbostratus, Stratus). Optically thick clouds had variability in τ_{atm} comparable to that of aerosol conditions, which was far lower than that of optically thinner clouds. Aerosol conditions marginally increased f_{dif} ($f_{dif} = 0.35$) relative to clear-sky conditions ($f_{dif} < f_{dif\_cs} + 0.1$) while barely reducing PAR. f_{dif} progressively increased with cloud optical thickness and approached 1 under intermediately thick clouds. Variability in f_{dif} was generally low, except under optically thin clouds.

To investigate $ADFE_t$ occurrence per cloudiness type, we selected combinations of f_{dif} and τ_{atm} for cloudy moments ($f_{dif} > f_{dif\_cs} + 0.1$) where GPP fell within the IQR of clear-sky GPP (Fig. 10; yellow line). On average, aerosol conditions and thin clouds caused combinations of f_{dif} and τ_{atm} that would be sufficient to reach clear-sky GPP rates. This was also true for intermediately thick clouds, perhaps with the exception of Altostratus. Optically thick clouds caused combinations of f_{dif} and τ_{atm} that seemed unlikely to result in a GPP equal to clear-sky GPP, let alone causing $ADFE_t$.

Finally, we determined how often $ADFE_t$ occurred under different cloudiness types (Fig. 10; inset): this was most often under aerosol conditions (55 % of the time that weather was classified as “aerosol”), followed by optically thin clouds (27–53 %) and never under optically

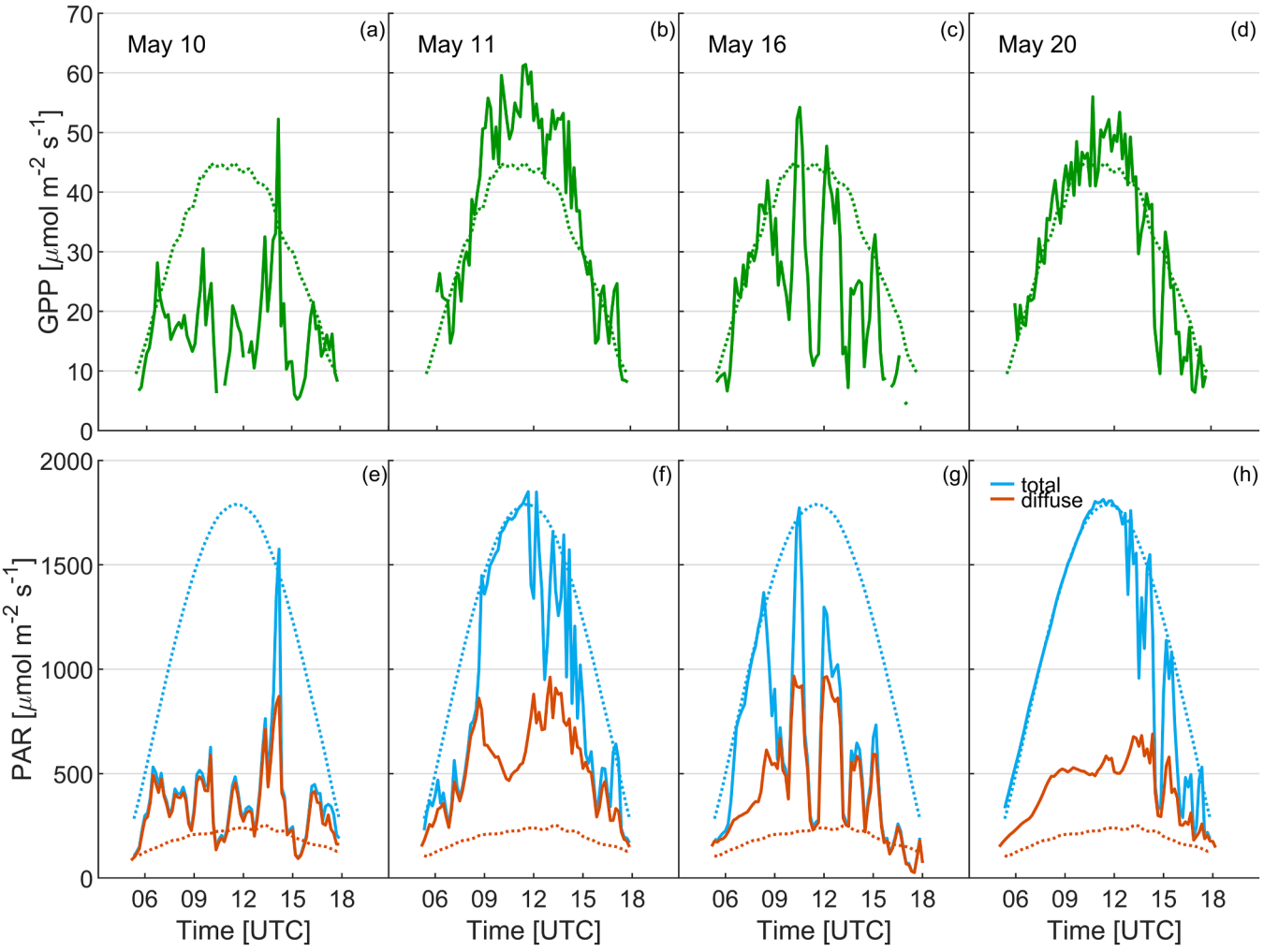

Fig. 6. Diurnal time courses of 10-minute GPP (a-d) and PAR (e-h), including the clear-sky reference day (dotted) and multiple days with cloudiness (solid) within the study period. Panels b and f show data of a day that showed ADFE in its daily GPP sum. Abbreviations: GPP, gross primary productivity; PAR, photosynthetically active radiation (top of canopy).

thick clouds. Unexpectedly, clouds of intermediate optical thickness caused $ADFE_t$ much less often (14–19 %) than optically thin clouds, while both cloud classes showed f_{dif} and τ_{atm} near those of clear-sky GPP equivalent. Overcast weather virtually always (>99 % of the time) reduced GPP, whereas under variable weather conditions GPP was reduced as often as increased compared to clear-sky GPP (not shown). $ADFE_t$ amplitude was largest under Cumulus (17 %) and smallest under Altocumulus (4 %; Table 1), although differences across cloudiness types were small compared to absolute GPP rates. More statistics per cloudiness type can be found in Table 1.

CE was present during 26 % of $ADFE_t$ periods: this was the case most often under Cumulus clouds and least under aerosol conditions, as reflected by variabilities in f_{dif} and τ_{atm} for these cloudiness types (Fig. 10). CE amplitudes were largest for Cumulus and Altostratus clouds, which likely caused CE to co-occur with $ADFE_t$ under these cloud types. Overall, we saw the fraction of time CE occurred increase from periods of GPP loss to periods of $ADFE_t$ (0.07 to 0.34; Fig. S3). However, especially the fraction of time shadow occurred reduced across the GPP classes (0.79 to 0.15) and was replaced by sunshine and CE.

4.3. Site characteristics and PDFE

Using the A_{can} model, we explored how site characteristics influenced the PDFE. The PDFE was positive irrespective of time of day or model scenario (Fig. 11; with the exception of the LAI = 1 scenario at dawn and dusk). The PDFE was larger in the morning than in the afternoon at equal PAR, as in the afternoon modelled GPP for the clear-sky and clear-sky perturbed simulations were higher than in the morning (Section 3.2.3). At dawn and dusk, PDFE decreased in all model scenarios due to increasing clear-sky f_{dif} (Fig. 3b). The PDFE changed mostly with LAI (Fig. 11a), canopy nitrogen distribution (Fig. 11c), LIAD (Fig. 11d), and leaf transmittance (Fig. 11f), and less so with latitude (Fig. 11b) and leaf reflectance (Fig. 11e).

The PDFE increased with LAI at any time of day. This increase was largest around dusk and dawn, and smallest at solar noon. The PDFE changed little with canopy nitrogen distribution at solar noon, but substantially at dawn and dusk. The PDFE varied differently with LIADs depending on time of day. Using a horizontal LIAD, the PDFE was low at dawn and dusk, and highest at solar noon. An opposite relation between PDFE and time of day occurred using a vertical LIAD, although the variation was less strong. PDFE variation in the spherical LIAD scenario was a balance of the PDFE variations in the horizontal and vertical LIAD scenarios. PDFE in the conical LIAD scenarios at 15° and 75° mimicked closely the PDFE in the horizontal and vertical LIAD scenarios, respectively.

5. Discussion

We addressed the current inability to explain variation in DFE occurrence across observational sites, hypothesizing that this inability is

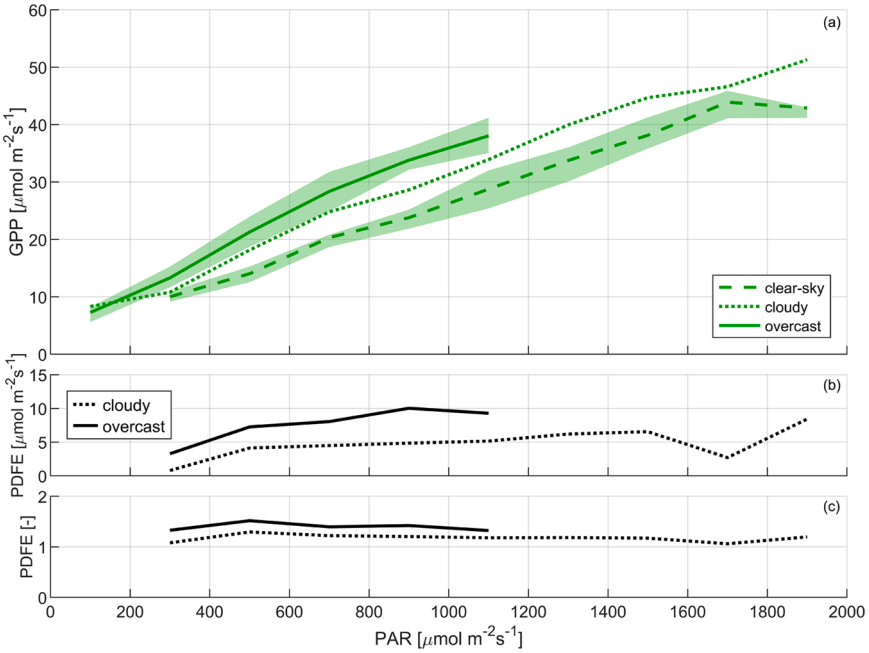

Fig. 7. Observed canopy LRCs and derived PDFE using observations from the entire study period. LRCs under clear-sky, cloudy, and overcast conditions (a). Differences in GPP (i.e. PDFE) between the overcast and clear-sky canopy LRCs (solid) and cloudy and clear-sky canopy LRCs (dotted) in absolute and relative units (b and c, respectively). Lines in (a) show medians of GPP, shaded areas indicate IQR (IQR of cloudy canopy LRC omitted for better visibility); clear-sky data match those in Fig. 3c. Panel a is an adaptation from Vilà-Guerau De Arellano et al. (2020; their Fig. 10a). Clear-sky, cloudy, and overcast conditions were selected through f_{dif}: clear-sky ($f_{dif} < f_{dif\_cs} + 0.1$), cloudy ($f_{dif} > f_{dif\_cs}$ + 0.1–0.7) and overcast ($f_{dif} > f_{dif\_cs} + 0.7$). Abbreviations: GPP, gross primary productivity; PAR, photosynthetically active radiation (top of canopy); PDFE, potential diffuse fertilization effect.

related to: (i) inconsistency in the definition and quantification of the DFE, (ii) the unexplored relation between DFE and cloudiness type, and (iii) insufficient knowledge on how various site characteristics affect DFE. For (i), we analysed how the literature defines and quantifies the DFE, and then developed and applied new guidelines for quantifying DFE from observations. For (ii) we analysed simultaneous observations of GPP, solar radiation and cloudiness types. For (iii) we tested the sensitivity of the DFE to various site characteristics using a canopy photosynthesis model. We found that visualisations of the DFE in the literature did not connect to existing definitions of the DFE or did not quantify the DFE with its causal factor sufficiently isolated. Furthermore, we found that DFE varies with both cloudiness type and site characteristics, thus characterizing two important and understudied sources of DFE variation.

In Section 5.1 we discuss the application of our guidelines to observational datasets (RQ1). In Section 5.2 we discuss variation in ADFE across cloudiness types (RQ2). In Section 5.3, we discuss variation in PDFE across site characteristics (RQ3).

5.1. Quantification of the DFE

The guidelines for quantifying the DFE focus on isolating the response of GPP to cloudiness (ADFE) or to f_{dif} (PDFE). Below we discuss four key challenges in applying these guidelines across different sites and conditions.

The first challenge is how one classifies a situation as being clear-sky. The perfect clear-sky would be an atmosphere without aerosols or clouds. Since there are always some aerosols present, such criterion would yield zero sample size from observations. Then it must be decided what aerosol concentration is still acceptable to label a situation as clear-sky. We used the minimum observed f_{dif} for each time of day, plus 0.1, as definition for a clear-sky. The use of a variable (with time-of-day) f_{dif}-threshold instead of the common fixed f_{dif}-threshold is an important improvement (Appendix A). The addition of 0.1 above the observed minimum is an arbitrary choice, which at our site yielded sufficient sample size and ensured that for instance hygroscopic aerosols events were separated from 'true' clear-sky moments. Ezhova et al. (2018) found that typical variation in aerosol load caused f_{dif} to vary between 0.1 and 0.2 at four high-latitude sites. If this result applies more widely, the addition of 0.1 at our site would have separated typical aerosol loads from more excessive aerosol loads as well. Yet, other sites may have different background aerosol loads, which may force to adjust the clear-sky demarcation in f_{dif} somewhat.

The next challenge is to define the pair of observations used to quantify the effect of cloudiness on GPP. In this study, we quantified $ADFE_t$ by comparing clear-sky and cloudy GPP at equal time-of-day across days within the study period (option 2 in Section 2.1.2). The alternative, comparing two moments on a given day following one another in time (option 1), yielded very few data pairs. The largest issue was that f_{dif} rarely met the clear-sky criterion on days with cloudiness. One reason may be the scattering of direct radiation by clouds onto the land surface, causing f_{dif} to increase even when clouds did not directly block the sun relative to the PAR sensor. For quantifying $ADFE_t$, option 1 has the benefit that it removes day-to-day variation in weather conditions more neatly, but it may not yield a sufficient sample size to be applied systematically across observational sites. To our knowledge, option 1 has not been applied previously except by comparing daily sums of GPP between consecutive days (Alton, 2008; Han et al., 2019; Hollinger et al., 1994), as was done in this study (Fig. 5).

Third, there is the challenge to find the right length of the dataset to be analysed. The analysis period must balance minimizing the temporal variability in site characteristics against capturing sufficient variation in clear and cloudy conditions. In our case, the study period of two weeks allowed us to quantify ADFE based on observations from multiple days, at constant time-of-day (solar elevation) and to capture sufficient variation in cloud types. An even shorter study period could have been preferable in our case, since crops have a relatively fast phenology. However, to capture the variation of ADFE over cloud types, we did need the full two-week period. Another aspect, in particular relevant for the determination of the PDFE, is that we could use 10-min averaged fluxes

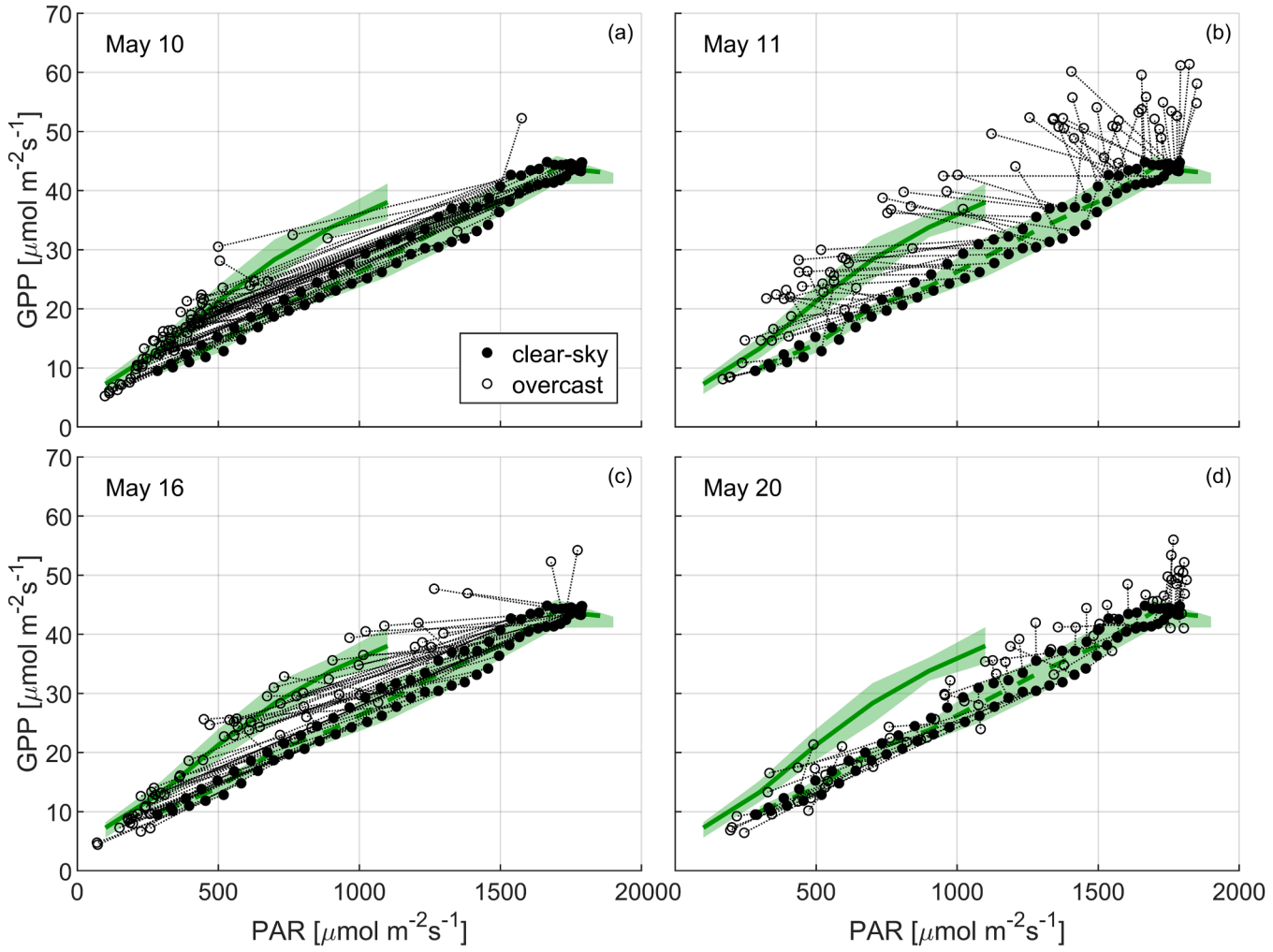

Fig. 8. Actual diffuse fertilization in relation to the potential diffuse fertilization effect during selected days. Open circles show 10-minute average observations, closed circles show observation-derived clear-sky conditions (see Fig. 3c). To indicate the relation between a given observation and its clear-sky counterpart, the open and closed circles that refer to the same time-of-day are connected by a line. Whenever an open circle is above the connected closed circle, ADFE is positive. Occurrence of ADFE relies on canopy LRCs for clear and cloudy conditions (clear sky: dashed green line, overcast: solid green line). Note that the selected days include mostly cloudy moments of various f_{dif}, but also some clear-sky moments (i.e. $f_{dif} < f_{dif\_cs} + 0.1$). Abbreviations: GPP, gross primary productivity; PAR, photosynthetically active radiation (top of canopy).

Table 1
Overview of key traits per weather class and cloud type (from left to right): occurrence frequency (f_{time}), atmospheric transmissivity (τ_{atm}), diffuse fraction (f_{dif}), fraction of time an ADFE occurred (f_{ADFE}), fraction of time cloud enhancement (CE) occurred (f_{CE}), fraction of ADFE time that CE occurred (f_{ADFE_CE}), amplitude of ADFE ($ADFE_{amp}$), and amplitude of CE (CE_{amp}). Occurrence frequencies for weather classes and for cloud types each add up to 1, and are expressed as fraction of total daytime ($\beta > 10°$) and total cloud detection time, respectively. CE_{amp} was calculated as the ratio of observed $S^{\downarrow}$ to clear-sky $S^{\downarrow}$ under CE. Thick clouds did not always correspond to overcast weather given the 60-minute time window restriction of the latter. All values represent medians of data. Abbreviations: ADFE, actual diffuse fertilization effect.

Weather class	f_{time} (-)	τ_{atm} (-)	f_{dif} (-)	f_{ADFE} (-)	f_{CE} (-)	f_{ADFE_CE} (-)	$ADFE_{amp}$ (-)	CE_{amp} (-)
Clear-sky	0.20	0.75	0.19	0	0	0	–	–
Variable	0.16	0.65	0.59	0.36	0.38	0.48	1.11	1.14
Overcast	0.19	0.17	1	0	0	0	–	–
No class assigned	0.33	0.49	0.74	0.32	0.14	0.28	1.10	1.12
Aerosol	0.12	0.72	0.35	0.55	0.06	0.07	1.11	1.05
Cloud type								
Altocumulus	0.08	0.65	0.58	0.27	0.20	0.31	1.04	1.08
Cirrus	0.19	0.66	0.58	0.53	0.17	0.30	1.10	1.13
Cumulus	0.11	0.50	0.87	0.42	0.28	0.47	1.17	1.19
Cirrostratus	0.10	0.39	0.98	0.14	0.01	0.12	1.10	1.09
Altostratus	0.07	0.34	0.97	0.17	0.11	0.38	1.08	1.25
Stratocumulus	0.19	0.39	0.99	0.19	0.10	0.32	1.10	1.16
Nimbostratus	0.07	0.23	1	0	0	0	–	–
Cumulonimbus	0.14	0.13	1	0	0	0	–	–
Stratus	0.05	0.14	1	0	0	0	–	–

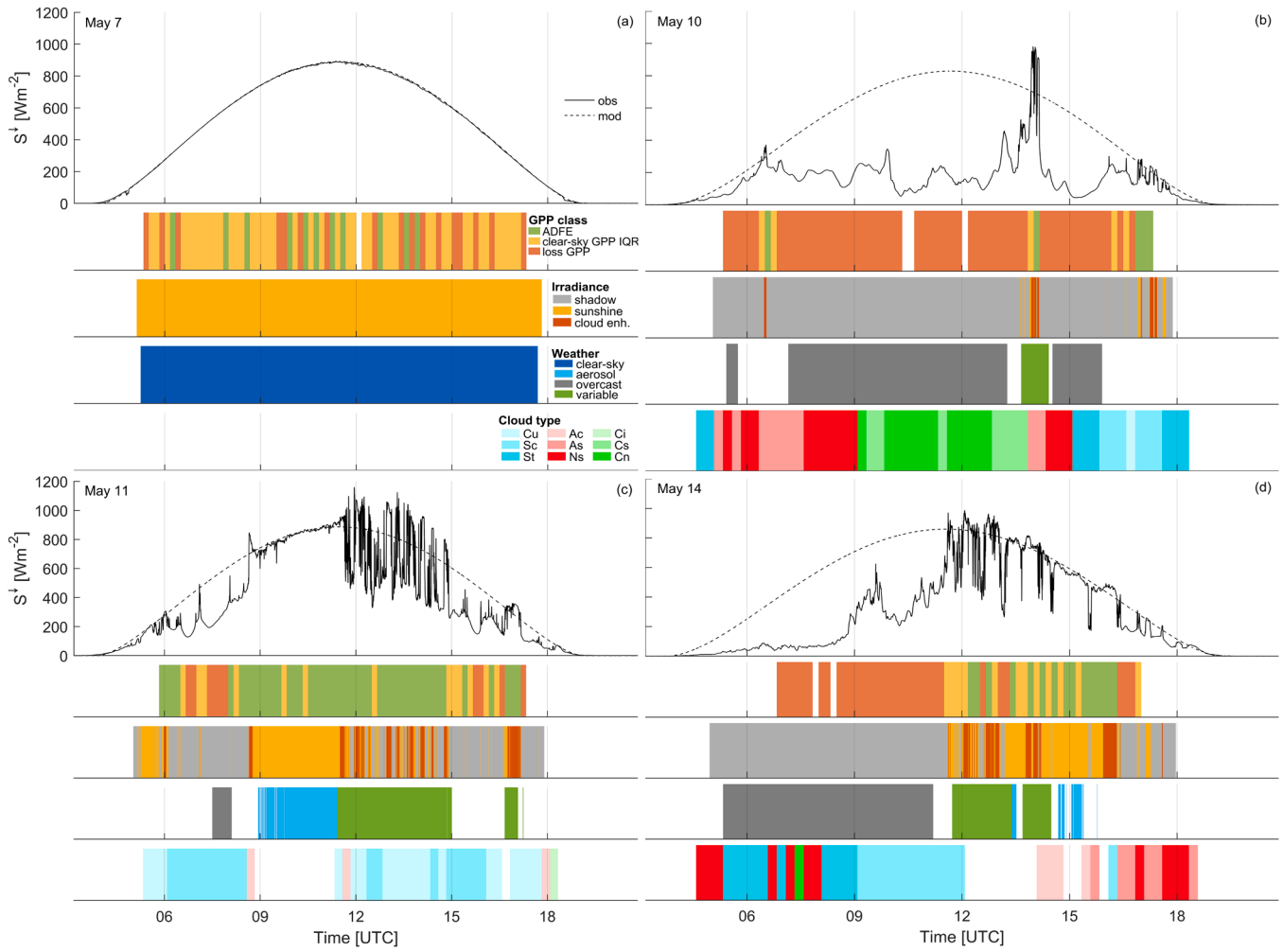

Fig. 9. Diurnal variation in global radiation ($S^{\downarrow}$) and conditions related to GPP, irradiance, weather and cloud type for four example days. Cloud type abbreviations: Cu, cumulus; Sc, Stratocumulus; St, Stratus (in cyan); Ac, Altocumulus; As, Altostratus; Ns, Nimbostratus (in red); Ci, cirrus; Cs, Cirrostratus; Cn, Cumulonimbus (in green). Abbreviations: IQR, interquartile range. Abbreviations: GPP, gross primary productivity.

of NEE instead of 30-min averages. As a result, the 10-min intervals often had a distinctive cloudy or clear-sky signature, and the sample size to construct the canopy LRCs was sufficient for robust statistics over the whole range of PAR. However, the use of 10-min averaged NEE fluxes at forested sites may not be justified given the larger height of the EC system (and related longer time scales). Yet, sample size at forested sites may be increased by selecting a longer study period, which would be justified to some extent given the typically slower phenology of forests as compared to crops.

Finally, a challenge in quantifying of the PDFE from observations in the summer is the strong asymmetry between morning and afternoon air temperature and VPD during clear-sky days. This asymmetry is thought to cause the observed asymmetry in GPP between morning and afternoon on those days, with the controlling mechanism being the closure of stomata in response to afternoon warming and drying of the atmospheric boundary layer (Lin et al., 2019; Pettigrew et al., 1990; Urban et al., 2012; Zhou et al., 2014). The median clear-sky GPP at a given PAR could be affected by this asymmetry, such that quantifying the PDFE separately for morning and afternoon should be considered. The immediate complication would be the halved sample sizes of the clear-sky and cloudy GPP pools, which leads back to the discussion of the third challenge. Our study period included moderate values for maximum clear-sky air temperature (25 °C) and VPD (2.2 kPa), with clear-sky GPP being 6–22 % lower in the afternoon than in the morning depending on PAR. The asymmetry in overcast GPP was smaller (1–15 %), and was more determined by day-to-day variation in GPP rather than by morning vs. afternoon effects, as our study period lacked a full overcast day. Thus, the exact influence of air temperature and VPD asymmetry on PDFE is uncertain for our study period, but may have been in the order of 10 %. In the modelled PDFE we circumvented this issue as it was determined as a function of time of day. For the same reason, there is no consequence regarding the quantification of the ADFE. Yet, ADFE on hot, dry days may more strongly depend on secondary cloud effects (i.e. changes in air temperature and VPD through changes in solar radiation) than on changes in total PAR and f_{dif} itself. Furthermore, the high ADFE occurrence under thin clouds as compared to thicker clouds that was found in our study period may reduce on such days, as air temperature and VPD remain high under thin clouds relative to thicker clouds.

Our dataset included both total PAR and diffuse PAR, allowing us to properly analyse PDFE and ADFE. To reduce uncertainty in the quantification of PDFE and ADFE, we strongly advise to use observations of f_{dif} and PAR (rather than global radiation). PAR is regularly estimated by applying a literature-based ratio of PAR to global radiation to observed global radiation. However, this ratio is not constant (Akitsu et al., 2015), and can introduce relative errors in estimated PAR up to 15 % (Akitsu et al., 2022). In addition, international EC data portals such as the European Integrated Carbon Observation System (Franz et al., 2018) or the global FluxNet2015 dataset (Pastorello et al., 2020) should aim to observe f_{dif} and PAR systematically. Unfortunately, currently less than 20 % of FLUXNET sites measure diffuse radiation (Zhou et al., 2021b).

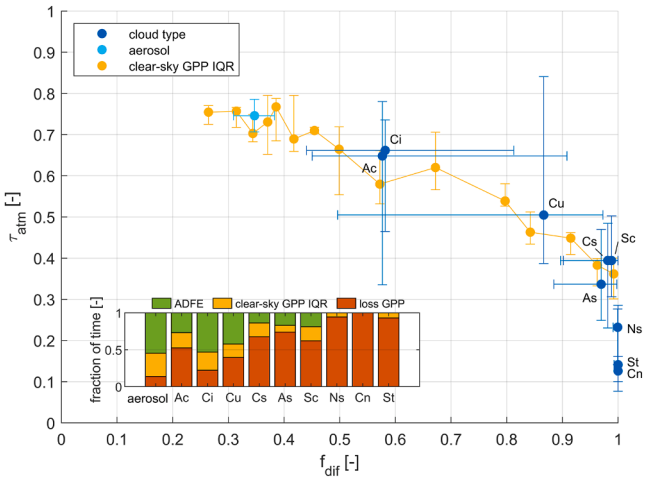

Fig. 10. Relationship between atmospheric transmissivity (τ_{atm}) and diffuse fraction of PAR (f_{dif}) under different cloudiness types. The yellow line represents cloudy moments ($f_{dif} > f_{dif\_cs} + 0.1$), of any cloudiness type, for which GPP fell within the IQR of clear-sky GPP. Symbols show medians ± IQRs. Inset: Fraction of occurrence of GPP classes (ADFE, clear-sky GPP IQR and loss GPP) across cloudiness types. Here, the observed GPP time series was cut up thrice: (i) GPP of cloudy moments ($f_{dif} > f_{dif\_cs} + 0.1$) were selected, (ii) GPP of cloudy moments were divided among cloudiness types, (iii) GPP of cloudy moments per cloudiness type were divided into the above-mentioned GPP classes. The occurrence frequency of cloudiness types can be found in Table 1. Abbreviations: GPP, gross primary production; IQR, interquartile range; ADFE, actual diffuse fertilization effect; Ac, altocumulus; Ci, cirrus; Cu, cumulus; Cs, cirrostratus; As, altostratus; Sc, stratocumulus; Ns, nimbostratus; Cn, cumulonimbus; St, stratus.

5.2. ADFE and cloudiness types

Numerous studies report that peak GPP is reached under intermediate f_{dif} (see references under GPP-f_{dif} in Table S1). Although $ADFE_t$ cannot be quantified from published GPP-f_{dif} relationships (Section 2.1.1), peak GPP at intermediate f_{dif} (Fig. 1a) implies the presence of $ADFE_t$. Intermediate f_{dif} would correspond to cloudiness with a cloud optical thickness (COT) <7 (Cheng et al., 2016; Pedruzo-Bagazgoitia et al., 2017), which in this study corresponds to aerosol conditions, thin clouds (COT <3.55) or intermediately thick clouds (COT 3.55–22.63). Most $ADFE_t$ at our site is caused under intermediate f_{dif} and low COT (aerosol, Cirrus, Altocumulus, Cumulus), confirming earlier results. However, clouds of intermediate thickness, despite average f_{dif} being close to 1 and average COT >7 (not shown), caused $ADFE_t$ often as well.

In fact, based on their f_{dif} and τ_{atm} (Fig. 10), clouds of intermediate thickness were expected to cause $ADFE_t$ as often as aerosol conditions or thin clouds, but this was not the case. We attempted to explain this using our canopy photosynthesis model: GPP increased with increasing f_{dif} at any PAR, but the magnitude of that increase became smaller with increasing f_{dif} (Fig. S4). In accordance with Lee et al. (2018), the cause for that is twofold: (i) shaded leaf area receives more PAR with increasing f_{dif}, but the additional GPP diminishes with increasing f_{dif} due to the curvilinearity of the leaf LRC, and (ii) sunlit leaf area receives less PAR with increasing f_{dif}, and the resulting loss in GPP becomes larger with increasing f_{dif} again due to the curvilinearity of the leaf LRC. Thus, a redistribution of PAR across the canopy leaf area following an increase in f_{dif} is most beneficial to GPP at low f_{dif}. Therefore, the PDFE under intermediately thick clouds is not much larger than under thin clouds, despite a large difference in f_{dif}. If PAR reduces proportionally with increasing f_{dif}, aerosol conditions and thin clouds clearly benefit GPP more than intermediate thick clouds do.

By combining satellite-based cloud classification with GPP, we related specific cloud types to $ADFE_t$ (Figs. 9 and 10; Table 1). We found contrasting results in solar radiation properties and $ADFE_t$ across thin clouds, which may be explained by their appearance. Cumulus and Altocumulus clouds appear as cloud fields with gaps of clear-sky, causing a bimodal distribution in solar radiation including frequent transitions between shadow and CE (Gristey et al., 2020; Mol et al., 2024; Schmidt et al., 2009, 2007; Tijhuis et al., 2023). In line with that, we observed high variability in f_{dif} and τ_{atm} under these cloud types. Additionally, Cumulus and Altocumulus clouds often caused CE and therefore corresponded often to variable weather and CE-induced $ADFE_t$. Cirrus, on the other hand, typically appears as a thin veil with a much larger horizontal than vertical dimension and causes weak, long-lasting CEs and shadows with low variability in solar radiation (Dowling and Radke, 1990; Kärcher, 2017; Mecikalski et al., 2013; Mol et al., 2023b). Cirrus clouds at our site indeed caused low variability in $S^{\downarrow}$ and corresponded infrequently to variable weather. Yet, CE was regularly present under Cirrus clouds. Additionally, we observed a variability in τ_{atm} and f_{dif} under Cirrus clouds comparable to that of Cumulus and Altocumulus. The reason for these deviating observations may be that high-altitude Cirrus clouds often co-occur with low-altitude Cumulus and Altocumulus clouds (Chang and Li, 2005; Mecikalski et al., 2013; Min et al., 2011). Since the cloud classification algorithm makes use of cloud top height, it may label a case as Cirrus clouds while Cumulus and Altocumulus clouds are also present (Mol et al., 2023b). Low-altitude clouds may be underrepresented at our site and the observed τ_{atm} and f_{dif} under Cirrus clouds may be biased. Biases may exist for Cumulus, Altocumulus, Altostratus and Cirrostratus, as these clouds tend to coexist as well (Li et al., 2015). Through visual inspection of our webcam footage, we detected regular cases of multi-layer cloud systems (Fig. S5). Globally, these occur 10–50 % of the time (Li et al., 2015), thus posing a complication to the satellite-based cloud classification algorithm here.

The varying occurrence of $ADFE_t$ across clouds of different COT as well as cloud types of equal COT implies that cloud types should be distinguished in global climate models. τ_{atm} and f_{dif} need to be accurately represented under various cloudiness conditions, since their combination is essential to GPP. Currently, only 6 out of 20 global vegetation models distinguish incoming solar radiation into its direct and diffuse components (Friedlingstein et al., 2023; their Table S1), causing the predicted global land sink of CO_2 to disregard an essential determinant of GPP. Variability in τ_{atm} and f_{dif}, including aspects like CE, is necessary for accurate prediction of GPP as well, since time-averaged values of solar radiation components lead to systematic GPP overestimation given the variable slope of the leaf LRC (Naumburg and Ellsworth, 2002). Aside from clouds, aerosol conditions may need to be distinguished into types as well in global climate models as different aerosol types can change τ_{atm} and f_{dif} differently (Durand et al., 2021; Li et al., 2025), and may affect ADFE differently (Harenda et al., 2022).

Given the large variability in surface solar radiation components under Cumulus and Altocumulus clouds (and to some extent under Altostratus and Stratocumulus), these cloud types may be the most relevant to photosynthesis under dynamically changing PAR (Burgess et al., 2023; Kaiser et al., 2018; Long et al., 2022; Slattery et al., 2018). Time-integrated GPP of crops may be lowered, potentially reducing crop yields, under fluctuating solar radiation that causes A_{can} to respond slowly (Deans et al., 2019; Kaiser et al., 2017; Long et al., 2022). Genetic manipulation or breeding of crops to respond to such fluctuations may enhance crop yields most strongly where these cloud types are abundant, although a more thorough analysis is needed on the temporal characteristics of PAR under these clouds in relation to the temporal characteristics of processes controlling A_{can}.

5.3. PDFE and site characteristics

Our model predicted the PDFE to be positive at all times of day across model scenarios. This was owed to the assumption that diffuse PAR spreads equally over the leaf area in a given canopy layer, whereas direct PAR illuminates only a fraction of that leaf area. That assumption leans

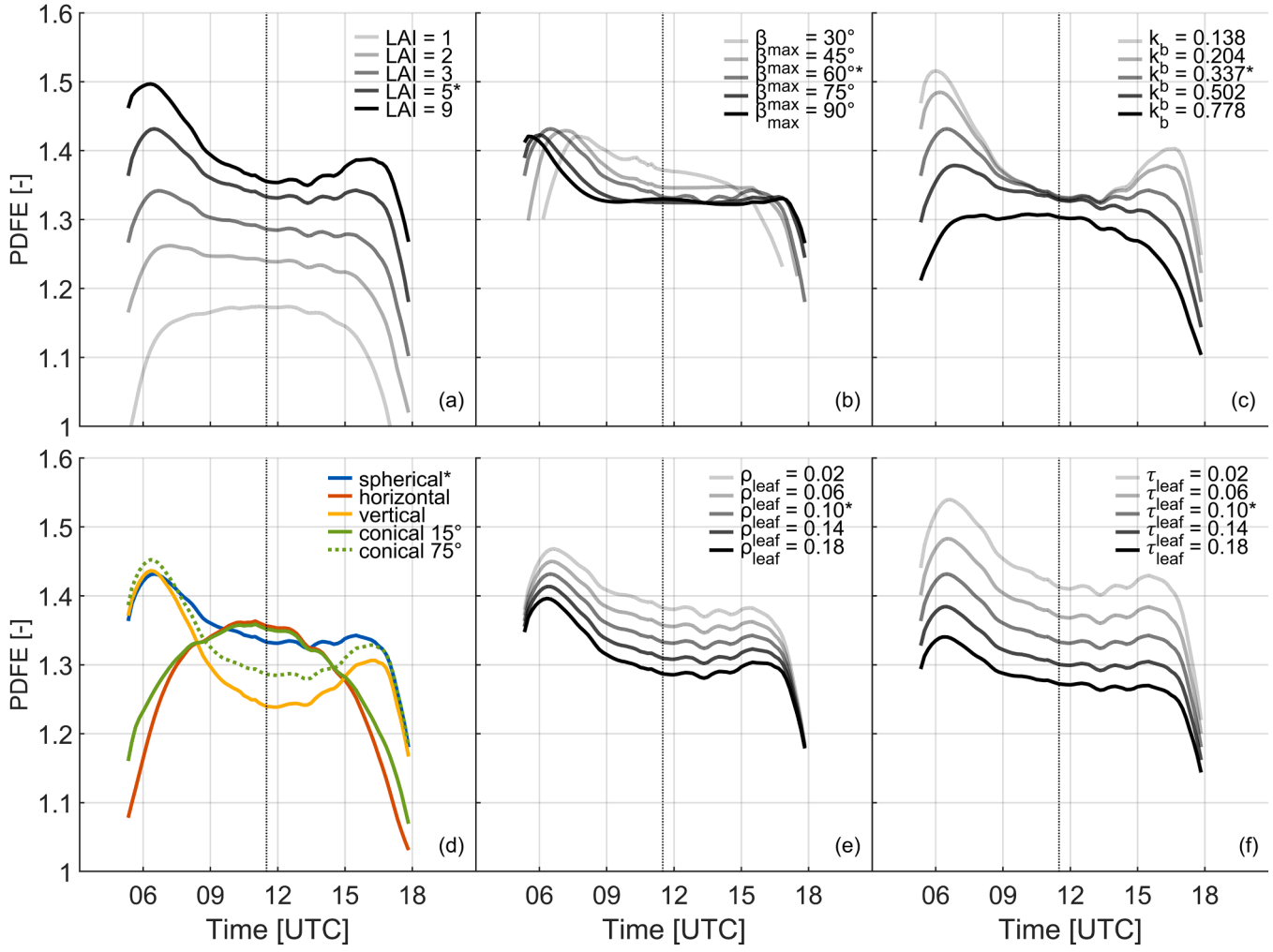

Fig. 11. Modelled diurnal time courses (β >10°) of the potential diffuse fertilization effect (PDFE) under different conditions in site characteristics: leaf area index (a), latitude expressed by β at solar noon (b), canopy nitrogen distribution expressed by the leaf nitrogen distribution coefficient (c), leaf inclination angle distribution (d), leaf reflectance (e), and leaf transmittance (f). Vertical dotted bars indicate solar noon. Asterisks indicate values representative for our site (i.e. default scenario), thus yielding equal diurnal PDFE. Small hiccups around 14:00 UTC were caused by systematic hiccups in measured clear-sky diffuse PAR (see Fig. 3b). Daytime varied for latitude scenarios as β was variable. Abbreviations: LAI, leaf area index.

on the principle that, contrary to 1D direct radiation, diffuse radiation is three-dimensional and therefore may illuminate each leaf at a given canopy depth with equal ease. The theory has been put forward that the DFE emerges from differences in mean profiles of direct and diffuse radiation (Urban et al., 2006, 2012; Zhao et al., 2023). Our model scenarios contradict that theory since a positive PDFE primarily emerged from a change in radiation distribution among leaves within a canopy layer, not from a change in mean radiation profiles. This result agrees with Williams et al. (2014), who did not observe a change in mean radiation profiles under varying f_{dif} but a change in radiation distribution horizontally across leaves.

Furthermore, in all model scenarios, the PDFE decreased at dawn and dusk primarily due to the increasing clear-sky f_{dif} (see Fig. 3b). The decreasing PDFE at increasing f_{dif} is not obvious since f_{dif} in the perturbed clear-sky simulation is always 0.7 above the default clear-sky simulation. Yet, we found that the benefit of an increase in f_{dif} to GPP, at any given PAR, decreases at higher f_{dif} (see Section 5.2). The PDFE decreased at dawn and dusk as well due to a decreasing PAR (Fig. 3b), which caused the LUE of saturated sunlit leaves under direct PAR to increase faster than the LUE of less-saturated leaves under diffuse PAR. However, the magnitude (and sign) of this effect depends on LIAD. Variation in PDFE across time of day per site characteristic are further discussed in Appendix I.

Our model results indicate that the PDFE is more sensitive to LAI, canopy nitrogen distribution, LIAD and leaf transmittance than to latitude or leaf reflectance. Since the PDFE can be quantified from observations with limited accuracy (see Section 2.1.2), and observing the isolated response of PDFE to a given site characteristic is impossible, more modelling studies are needed for comparison to our results. Knohl and Baldocchi (2008) simulated that diurnally averaged PDFE was more sensitive to leaf transmission than to leaf reflection or leaf orientation, although using diurnally averaged PDFE may confound comparison between site characteristics (see Appendix I). At our site, $ADFE_t$ may have been facilitated most by LAI and LIAD, given their specifics (5 m^2 m^{-2} and "spherical") would have increased the PDFE relative to other sites (Fig. 11a,d). Leaf transmittance was not observed here, so we are not able to discuss its effect on $ADFE_t$. Canopy nitrogen distribution of the canopy at our site was average compared to the natural range (Fig. 11c), so it may not have facilitated $ADFE_t$ more than it would at other sites.

6. Conclusions

We addressed the inability to explain variation in DFE occurrence across observational sites. We hypothesized that this inability is related to: (i) inconsistency in the definition and quantification of the DFE, (ii)

the unexplored relation between DFE and cloudiness type, and (iii) insufficient knowledge on how site characteristics affect DFE. These hypotheses corresponded to three research questions (RQ1, RQ2 and RQ3), respectively.

For RQ1 we showed that: (a) different DFE definitions exist, (b) the DFE is quantified such that a connection to existing definitions is not possible or that the causal factor of the DFE is not isolated, (c) there is no systematic protocol used to quantify DFE. In response to (b) and (c), we proposed two guidelines that can be applied systematically across studies and aim to isolate the causal factor of the DFE. For (a), we illustrated the relation between DFE definitions in a theoretical framework, which automatically served to qualitatively determine how the DFE varies with cloudiness types (RQ2) and site characteristics (RQ3). For RQ2 we applied our guidelines and framework to an observational dataset covering simultaneous observations of canopy photosynthesis, solar radiation, cloudiness types and site characteristics. We showed that the trade-off between diffuse radiation and total solar radiation varied under different cloudiness types, which likely explained the observed variation in DFE with cloudiness type. To our knowledge, we are the first to report observed DFE variation with cloudiness types. For RQ3, using an observation-driven canopy photosynthesis model, we showed variation in the DFE magnitude with site characteristics and time of day. The DFE magnitude was more sensitive to leaf area index, canopy nitrogen distribution, leaf orientation and leaf transmittance than to latitude or leaf reflectance. At our site, a high leaf area index and a spherical leaf orientation likely contributed most to DFE occurrences.

Our study emphasizes the importance of quantifying the DFE systematically and accurately across observational sites. Additionally, documentation of cloudiness climatology and site characteristics is needed to explain the full variation in DFE occurrence across sites.

Abbreviation list

ADFE: actual DFE.

$ADFE_{day}$: actual DFE based on a comparison of two daily GPP sums ($\mu mol(CO_2)\ m^{-2}day^{-1}$).

$ADFE_t$: actual DFE based on a comparison of two moments of equal time of day ($\mu mol(CO_2)\ m^{-2}s^{-1}$).

CE: cloud enhancement.

DFE: diffuse fertilization effect.

DFE_{GPP}: diffuse fertilization effect on GPP.

DFE_{LUE}: diffuse fertilization effect on canopy LUE.

EC: eddy covariance.

GPP: gross primary productivity ($\mu mol(CO_2)\ m^{-2}s^{-1}$).

$GPP_{ref,day}$: clear-sky reference daily GPP sum ($mol(CO_2)\ m^{-2}day^{-1}$).

IQR: interquartile range.

LAI: leaf area index (m^2(leaf) m^{-2}(ground)).

LIAD: leaf inclination angle distribution.

LUE: light use efficiency of the canopy.

LRC: light response curve.

NEE: net ecosystem exchange ($\mu mol(CO_2)\ m^{-2}s^{-1}$).

PAR: photosynthetic active radiation at the top of the canopy ($\mu mol(photon)\ m^{-2}s^{-1}$).

PDFE: potential DFE ($\mu mol(CO_2)\ m^{-2}s^{-1}$).

RT: radiative transfer.

$S^{\downarrow}$: global radiation at the top of the canopy (W m^{-2}).

$S^{\downarrow}_{TOA}$: global radiation at the top of the atmosphere (W m^{-2}).

VPD: vapor pressure deficit (Pa).

Data availability

The observational data and model scripts used to generate the results in this report are available at: 10.5281/zenodo.15332572.

CRediT authorship contribution statement

Kevin H.H. van Diepen: Writing – review & editing, Writing – original draft, Formal analysis. **Elias Kaiser:** Writing – review & editing. **Oscar K. Hartogensis:** Investigation. **Alexander Graf:** Investigation, Funding acquisition. **Jordi Vilà-Guerau de Arellano:** Supervision. **Arnold F. Moene:** Writing – review & editing, Conceptualization.

Declaration of competing interest

The authors declare that they have no known competing financial interests or personal relationships that could have appeared to influence the work reported in this paper.

Acknowledgments

This study was financed by the Deutsche Forschungsgemeinschaft (DFG) Collaborative Research Centre 32 (TR32) “Patterns in Soil-Vegetation-Atmosphere System”. KHHvD was further financed through a PhD-grant of the C.T. de Wit Graduate School for Production Ecology and Resource Conservation. The global radiation, PAR (one Li-190R, two BF5), and LAI observations used in this study are from the ICOS station DE-RuS, but have no DOI due to the fact that the field campaign took place during the labelling (ramp-up) phase as an ICOS class 1 station. We thank Marius Schmidt and Daniel Dolfus for operating the station and providing the data. We thank Jan Goudriaan for assistance with the development of the canopy photosynthesis model. We further thank Wouter Mol for assistance with the application and interpretation of the irradiance, weather and cloud classifications.

Supplementary materials

Supplementary material associated with this article can be found, in the online version, at doi:10.1016/j.agrformet.2025.110597.

References

Akitsu, T., Kume, A., Hirose, Y., Ijima, O., Nasahara, K.N., 2015. On the stability of radiometric ratios of photosynthetically active radiation to global solar radiation in Tsukuba, Japan. Agric. For. Meteorol. 209-210, 59–68. https://doi.org/10.1016/j.agrformet.2015.04.026.

Akitsu, T.K., Nasahara, K.N., Ijima, O., Hirose, Y., Ide, R., Takagi, K., Kume, A., 2022. The variability and seasonality in the ratio of photosynthetically active radiation to solar radiation: a simple empirical model of the ratio. Int. J. Appl. Earth Observ. Geoinf. 108. https://doi.org/10.1016/j.jag.2022.102724.

Alton, P.B., 2008. Reduced carbon sequestration in terrestrial ecosystems under overcast skies compared to clear skies. Agric. For. Meteorol. 148 (10), 1641–1653. https://doi.org/10.1016/j.agrformet.2008.05.014.

Alton, P.B., North, P.R., Los, S.O., 2007. The impact of diffuse sunlight on canopy light-use efficiency, gross photosynthetic product and net ecosystem exchange in three forest biomes. Glob. Change Biol. 13 (4), 776–787. https://doi.org/10.1111/j.1365-2486.2007.01316.x.

Arias, P., Bellouin, N., Coppola, E., Jones, R., Krinner, G., Marotzke, J., et al. (2021). Climate Change 2021: the physical science basis. Contribution of Working Group I to the Sixth Assessment Report of the Intergovernmental Panel on Climate Change; technical summary.

Bonan, G.B., Lawrence, P.J., Oleson, K.W., Levis, S., Jung, M., Reichstein, M., et al., 2011. Improving canopy processes in the Community Land Model version 4 (CLM4) using global flux fields empirically inferred from FLUXNET data. J. Geophys. Res. 116 (G2). https://doi.org/10.1029/2010jg001593.

Burgess, A.J., Masclaux-Daubresse, C., Strittmatter, G., Weber, A.P.M., Taylor, S.H., Harbinson, J., et al., 2023. Improving crop yield potential: underlying biological processes and future prospects. Food Energy Secur. 12 (1), e435. https://doi.org/10.1002/fes3.435.

Campbell, G., Norman, J., 1989. The description and measurement of plant canopy structure. In Plant Canopies: Their Growth, Form and Function. In: Russell, G. (Ed.), Society for Experimental Biology, Seminar Series, 29. Cambridge University Press, New York.

Campbell, G.S., Norman, J.M., 2000. An Introduction to Environmental Biophysics. Springer Science & Business Media.

Chakraborty, T., Lee, X., Lawrence, D.M., 2022. Diffuse radiation forcing constraints on gross primary productivity and global terrestrial evapotranspiration. Earth’s Fut. 10 (8). https://doi.org/10.1029/2022ef002805.

Chang, F.-L., Li, Z., 2005. A new method for detection of cirrus overlapping water clouds and determination of their optical properties. J. Atmosp. Sci. 62 (11), 3993–4009.

Chapin, F.S., Woodwell, G.M., Randerson, J.T., Rastetter, E.B., Lovett, G.M., Baldocchi, D.D., et al., 2006. Reconciling carbon-cycle concepts, terminology, and methods. Ecosystems 9 (7), 1041–1050. https://doi.org/10.1007/s10021-005-0105-7.

Cheng, S.J., Bohrer, G., Steiner, A.L., Hollinger, D.Y., Suyker, A., Phillips, R.P., Nadelhoffer, K.J., 2015. Variations in the influence of diffuse light on gross primary productivity in temperate ecosystems. Agric. For. Meteorol. 201, 98–110. https://doi.org/10.1016/j.agrformet.2014.11.002.

Cheng, S.J., Steiner, A.L., Hollinger, D.Y., Bohrer, G., Nadelhoffer, K.J., 2016. Using satellite-derived optical thickness to assess the influence of clouds on terrestrial carbon uptake. J. Geophys. Res.: Biogeosci. 121 (7), 1747–1761. https://doi.org/10.1002/2016jg003365.

Cirino, G.G., Souza, R.A.F., Adams, D.K., Artaxo, P., 2014. The effect of atmospheric aerosol particles and clouds on net ecosystem exchange in the Amazon. Atmosp. Chem. Phys. 14 (13), 6523–6543. https://doi.org/10.5194/acp-14-6523-2014.

Clark, D.B., Mercado, L.M., Sitch, S., Jones, C.D., Gedney, N., Best, M.J., et al., 2011. The joint UK land environment simulator (JULES), model description – Part 2: carbon fluxes and vegetation dynamics. Geosci. Model Dev. 4 (3), 701–722. https://doi.org/10.5194/gmd-4-701-2011.

Damour, G., Simonneau, T., Cochard, H., Urban, L., 2010. An overview of models of stomatal conductance at the leaf level. Plant Cell Environ. 33 (9), 1419–1438. https://doi.org/10.1111/j.1365-3040.2010.02181.x.

Deans, R.M., Brodribb, T.J., Busch, F.A., Farquhar, G.D., 2019. Plant water-use strategy mediates stomatal effects on the light induction of photosynthesis. New. Phytol. 222 (1), 382–395. https://doi.org/10.1111/nph.15572.

Denmead, O.T., 1991. Sources and sinks of greenhouse gases in the soil-plant environment. Vegetation 91 (1–2), 73–86. https://doi.org/10.1007/bf00036049.

Disney, M., 2016. Remote sensing of vegetation: potentials, limitations, developments and applications. Canopy Photosynthesis: from Basics to Applications. Springer, pp. 289–331.

Dowling, D.R., Radke, L.F., 1990. A summary of the physical properties of cirrus clouds. J. Appl. Meteorol. Climatol. 29 (9), 970–978.

Durand, M., Murchie, E.H., Lindfors, A.V., Urban, O., Aphalo, P.J., Robson, T.M., 2021. Diffuse solar radiation and canopy photosynthesis in a changing environment. Agric. For. Meteorol. 311. https://doi.org/10.1016/j.agrformet.2021.108684.

Ezhova, E., Ylivinkka, I., Kuusk, J., Komsaare, K., Vana, M., Krasnova, A., et al., 2018. Direct effect of aerosols on solar radiation and gross primary production in boreal and hemiboreal forests. Atmosp. Chem. Phys. 18 (24), 17863–17881. https://doi.org/10.5194/acp-18-17863-2018.

Farquhar, G.D., von Caemmerer, S.v., Berry, J.A., 1980. A biochemical model of photosynthetic CO_2 assimilation in leaves of C3 species. Planta 149, 78–90.

Feng, J., Zhang, B., Wei, Z., Xu, D., 2017. Effects of averaging period on energy fluxes and the energy-balance ratio as measured with an Eddy-covariance system. Boundary. Layer. Meteorol. 165 (3), 545–551. https://doi.org/10.1007/s10546-017-0284-8.

Foken, T., Göockede, M., Mauder, M., Mahrt, L., Amiro, B., Munger, W., 2004. Post-field data quality control. Handbook of Micrometeorology: a Guide for Surface Flux Measurement and Analysis 181–208.

Franz, D., Acosta, M., Altimir, N., Arriga, N., Arrouays, D., Aubinet, M., et al., 2018. Towards long-term standardised carbon and greenhouse gas observations for monitoring Europe's terrestrial ecosystems: a review. Int. Agrophys. 32 (4), 439–455. https://doi.org/10.1515/intag-2017-0039.

Friedlingstein, P., O'Sullivan, M., Jones, M.W., Andrew, R.M., Bakker, D.C.E., Hauck, J., et al., 2023. Global Carbon Budget 2023. Earth Syst. Sci. Data 15 (12), 5301–5369. https://doi.org/10.5194/essd-15-5301-2023.

Geerdt, M. (2007). Jan IngenHousz, or why don't we know who discovered photosynthesis?.

Gest, H., 2000. Bicentenary homage to Dr Jan Ingen-Housz, MD (1730–1799), pioneer of photosynthesis research. Photosyn. Res. 63, 183–190.

Goudriaan, J., 1977. Crop Micrometeorology: a Simulation Study. Wageningen University and Research.

Goudriaan, J., 2016. Light Distribution. In: Hikosaka, K., Niinemets, Ü., Anten, N. (Eds.), Canopy Photosynthesis: From Basics to Applications. Advances in Photosynthesis and Respiration. Springer, Dordrecht, p. 42. https://doi.org/10.1007/978-94-017-7291-4_1.

Goudriaan, J., Van Laar, H., 2012. Modelling Potential Crop Growth Processes: textbook with Exercises, Vol. 2. Springer Science & Business Media.

Grace, J., 1971. The directional distribution of light in natural and controlled environment conditions. J. Appl. Ecol. 8 (1), 155–164.

Gristey, J.J., Feingold, G., Glenn, I.B., Schmidt, K.S., Chen, H., 2020. On the relationship between shallow cumulus cloud field properties and surface solar irradiance. Geophys. Res. Lett. 47 (22). https://doi.org/10.1029/2020gl090152.

Gristey, J.J., Feingold, G., Schmidt, K.S., Chen, H., 2022. Influence of aerosol embedded in shallow cumulus cloud fields on the surface solar irradiance. J. Geophys. Res.: Atmosp. 127 (11). https://doi.org/10.1029/2022jd036822.

Gu, L., Baldocchi, D., Verma, S.B., Black, T.A., Vesala, T., Falge, E.M., Dowty, P.R., 2002. Advantages of diffuse radiation for terrestrial ecosystem productivity. J. Geophys. Res.: Atmosp. 107 (D6). https://doi.org/10.1029/2001jd001242.

Gu, L., Fuentes, J.D., Shugart, H.H., Staebler, R.M., Black, T.A., 1999. Responses of net ecosystem exchanges of carbon dioxide to changes in cloudiness: results from two North American deciduous forests. J. Geophys. Res.: Atmosp. 104 (D24), 31421–31434.

Gui, X., Wang, L., Su, X., Yi, X., Chen, X., Yao, R., Wang, S., 2021. Environmental factors modulate the diffuse fertilization effect on gross primary productivity across Chinese ecosystems. Sci. Total Environ. 793, 148443. https://doi.org/10.1016/j.scitotenv.2021.148443.

Han, J., Zhang, L., Li, S., Wen, X., Li, Q., Wang, H., 2019. Effects of sky conditions on net ecosystem productivity of a subtropical coniferous plantation vary from half-hourly to daily timescales. Sci. Total. Environ. 651 (Pt 2), 3002–3014. https://doi.org/10.1016/j.scitotenv.2018.10.190.

Harenda, K.M., Markowicz, K.M., Poczta, P., Stachlewska, I.S., Bojanowski, J.S., Czernecki, B., et al., 2022. Estimation of the effects of aerosol optical properties on peatland production in Rzecin, Poland. Agric. For. Meteorol. 316, 108861.

Hemes, K.S., Verfaillie, J., Baldocchi, D.D., 2020. Wildfire-smoke aerosols lead to increased light use efficiency among agricultural and restored wetland land uses in California's Central Valley. J. Geophys. Res.: Biogeosci. 125 (2). https://doi.org/10.1029/2019jg005380.

Hikosaka, K., Anten, N.P., Borjigidai, A., Kamiyama, C., Sakai, H., Hasegawa, T., et al., 2016. A meta-analysis of leaf nitrogen distribution within plant canopies. Ann. Bot. 118 (2), 239–247. https://doi.org/10.1093/aob/mcw099.

Hollinger, D., Kelliher, F., Byers, J., Hunt, J., McSeveny, T., Weir, P., 1994. Carbon dioxide exchange between an undisturbed old-growth temperate forest and the atmosphere. Ecology 75 (1), 134–150.

Ingenhousz, J. (1779). Experiments upon vegetables, discovering their great power of purifying the common air in the sun-shine, and of injuring it in the shade and at night: to which is joined, a new method of examining the accurate degree of salubrity of the atmosphere: P. Elmsly, and H. Payne.

Kaiser, E., Kromdijk, J., Harbinson, J., Heuvelink, E., Marcelis, L.F., 2017. Photosynthetic induction and its diffusional, carboxylation and electron transport processes as affected by CO2 partial pressure, temperature, air humidity and blue irradiance. Ann. Bot. 119 (1), 191–205. https://doi.org/10.1093/aob/mcw226.

Kaiser, E., Morales, A., Harbinson, J., 2018. Fluctuating light takes crop photosynthesis on a rollercoaster ride. Plant Physiol. 176 (2), 977–989. https://doi.org/10.1104/pp.17.01250.

Kalidindi, S., Bala, G., Modak, A., Caldeira, K., 2014. Modeling of solar radiation management: a comparison of simulations using reduced solar constant and stratospheric sulphate aerosols. Clim. Dyn. 44 (9–10), 2909–2925. https://doi.org/10.1007/s00382-014-2240-3.

Kanniah, K.D., Beringer, J., Hutley, L., 2013. Exploring the link between clouds, radiation, and canopy productivity of tropical savannas. Agric. For. Meteorol. 182-183, 304–313. https://doi.org/10.1016/j.agrformet.2013.06.010.

Kanniah, K.D., Beringer, J., North, P., Hutley, L., 2012. Control of atmospheric particles on diffuse radiation and terrestrial plant productivity. Progr. Phys. Geogr.: Earth Environ. 36 (2), 209–237. https://doi.org/10.1177/0309133311434244.

Kärcher, B., 2017. Cirrus clouds and their response to anthropogenic activities. Curr. Clim. Change Rep. 3 (1), 45–57. https://doi.org/10.1007/s40641-017-0060-3.

Knauer, J., Zaehle, S., De Kauwe, M.G., Haverd, V., Reichstein, M., Sun, Y., 2020. Mesophyll conductance in land surface models: effects on photosynthesis and transpiration. Plant J. 101 (4), 858–873. https://doi.org/10.1111/tpj.14587.

Knohl, A., Baldocchi, D.D., 2008. Effects of diffuse radiation on canopy gas exchange processes in a forest ecosystem. J. Geophys. Res.: Biogeosci. 113 (G2). https://doi.org/10.1029/2007jg000663.

Krinner, G., Viovy, N., de Noblet-Ducoudré, N., Ogée, J., Polcher, J., Friedlingstein, P., et al., 2005. A dynamic global vegetation model for studies of the coupled atmosphere-biosphere system. Glob. Biogeochem. Cycles 19 (1). https://doi.org/10.1029/2003gb002199.

Lasslop, G., Migliavacca, M., Bohrer, G., Reichstein, M., Bahn, M., Ibrom, A., et al., 2012. On the choice of the driving temperature for eddy-covariance carbon dioxide flux partitioning. Biogeosciences 9 (12), 5243–5259. https://doi.org/10.5194/bg-9-5243-2012.

Lasslop, G., Reichstein, M., Papale, D., Richardson, A.D., Arneth, A., Barr, A., et al., 2009. Separation of net ecosystem exchange into assimilation and respiration using a light response curve approach: critical issues and global evaluation. Glob. Change Biol. 16 (1), 187–208. https://doi.org/10.1111/j.1365-2486.2009.02041.x.

Lee, M.S., Hollinger, D.Y., Keenan, T.F., Ouimette, A.P., Ollinger, S.V., Richardson, A.D., 2018. Model-based analysis of the impact of diffuse radiation on CO2 exchange in a temperate deciduous forest. Agric. For. Meteorol. 249, 377–389. https://doi.org/10.1016/j.agrformet.2017.11.016.

Leuning, R., 1995. A critical appraisal of a combined stomatal-photosynthesis model for C3 plants. Plant Cell Environ. 18 (4), 339–355.

Li, J., Huang, J., Stamnes, K., Wang, T., Lv, Q., Jin, H., 2015. A global survey of cloud overlap based on CALIPSO and CloudSat measurements. Atmosp. Chem. Phys. 15 (1), 519–536. https://doi.org/10.5194/acp-15-519-2015.

Li, H., Zhang, M., Wang, L., Su, X., Lu, Y., 2025. Effects of different types of aerosols on diffuse radiation based on global AERONET. J. Geophys. Res. Atmos. 130 (5). https://doi.org/10.1029/2024JD042701.

Lin, C., Gentine, P., Frankenberg, C., Zhou, S., Kennedy, D., Li, X., 2019. Evaluation and mechanism exploration of the diurnal hysteresis of ecosystem fluxes. Agric. For. Meteorol. 278, 107642.

Liu, P., Tong, X., Zhang, J., Meng, P., Li, J., Zhang, J., Zhou, Y., 2022. Effect of diffuse fraction on gross primary productivity and light use efficiency in a warm-temperate mixed plantation. Front. Plant Sci. 13, 966125. https://doi.org/10.3389/fpls.2022.966125.

Long, S.P., Taylor, S.H., Burgess, S.J., Carmo-Silva, E., Lawson, T., De Souza, A.P., et al., 2022. Into the shadows and back into sunlight: photosynthesis in fluctuating light. Annu Rev. Plant Biol. 73, 617–648. https://doi.org/10.1146/annurev-arplant-070221-024745.

Mecikalski, J.R., Minnis, P., Palikonda, R., 2013. Use of satellite derived cloud properties to quantify growing cumulus beneath cirrus clouds. Atmosp. Res. 120-121, 192–201. https://doi.org/10.1016/j.atmosres.2012.08.017.

Mercado, L.M., Bellouin, N., Sitch, S., Boucher, O., Huntingford, C., Wild, M., Cox, P.M., 2009. Impact of changes in diffuse radiation on the global land carbon sink. Nature 458 (7241), 1014–1017. https://doi.org/10.1038/nature07949.

Min, M., Wang, P., Campbell, J.R., Zong, X., Xia, J., 2011. Cirrus cloud macrophysical and optical properties over North China from CALIOP measurements. Adv. Atmosp. Sci. 28 (3), 653–664. https://doi.org/10.1007/s00376-010-0049-5.

Moene, A.F., Van Dam, J.C., 2014. Transport in the Atmosphere-Vegetation-Soil Continuum. Cambridge University Press.

Mol, W., Heusinkveld, B., Mangan, M.R., Hartogensis, O., Veerman, M., van Heerwaarden, C., 2024. Observed patterns of surface solar irradiance under cloudy and clear-sky conditions. Q. J. R. Meteorol. Soc. 150 (761), 2338–2363. https://doi.org/10.1002/qj.4712.

Mol, W.B., Knap, W.H., van Heerwaarden, C.C., 2023a. Ten years of 1 hz solar irradiance observations at Cabauw, The Netherlands, with cloud observations, variability classifications, and statistics. Earth Syst. Sci. Data 15 (5), 2139–2151. https://doi.org/10.5194/essd-15-2139-2023.

Mol, W.B., van Stratum, B.J., Knap, W.H., van Heerwaarden, C.C., 2023b. Reconciling observations of solar irradiance variability with cloud size distributions. J. Geophys. Res.: Atmosp. 128 (5) e2022JD037894.

Naumburg, E., Ellsworth, D.S., 2002. Short-term light and leaf photosynthetic dynamics affect estimates of daily understory photosynthesis in four tree species. Tree Physiol. 22 (6), 393–401.

Niinemets, U., Diaz-Espejo, A., Flexas, J., Galmes, J., Warren, C.R., 2009. Role of mesophyll diffusion conductance in constraining potential photosynthetic productivity in the field. J. Exp. Bot. 60 (8), 2249–2270. https://doi.org/10.1093/jxb/erp036.

Oliphant, A.J., Dragoni, D., Deng, B., Grimmond, C.S.B., Schmid, H.P., Scott, S.L., 2011. The role of sky conditions on gross primary production in a mixed deciduous forest. Agric. For. Meteorol. 151 (7), 781–791. https://doi.org/10.1016/j.agrformet.2011.01.005.

Oliveira, P.H.F., Artaxo, P., Pires, C., De Lucca, S., Procópio, A., Holben, B., et al., 2007. The effects of biomass burning aerosols and clouds on the CO_2flux in Amazonia. Tellus B: Chem. Phys. Meteorol. 59 (3), 338–349. https://doi.org/10.1111/j.1600-0889.2007.00270.x.

Park, S.-B., Knohl, A., Lucas-Moffat, A.M., Migliavacca, M., Gerbig, C., Vesala, T., et al., 2018. Strong radiative effect induced by clouds and smoke on forest net ecosystem productivity in central Siberia. Agric. For. Meteorol. 250-251, 376–387. https://doi.org/10.1016/j.agrformet.2017.09.009.

Pastorello, G., Trotta, C., Canfora, E., Chu, H., Christianson, D., Cheah, Y.W., et al., 2020. The FLUXNET2015 dataset and the ONEFlux processing pipeline for eddy covariance data. Sci. Data 7 (1), 225. https://doi.org/10.1038/s41597-020-0534-3.

Pedruzo-Bagazgoitia, X., Ouwersloot, H.G., Sikma, M., van Heerwaarden, C.C., Jacobs, C. M.J., Vilà-Guerau de Arellano, J., 2017. Direct and diffuse radiation in the shallow cumulus–Vegetation system: enhanced and decreased evapotranspiration regimes. J. Hydrometeorol. 18 (6), 1731–1748. https://doi.org/10.1175/jhm-d-16-0279.1.

Pettigrew, W., Hesketh, J., Peters, D., Woolley, J., 1990. A vapor pressure deficit effect on crop canopy photosynthesis. Photosyn. Res. 24, 27–34.

Price, D., Black, T., 1990. Effects of short-term variation in weather on diurnal canopy CO2 flux and evapotranspiration of a juvenile Douglas-fir stand. Agric. For. Meteorol. 50 (3), 139–158.

Proctor, J., Hsiang, S., Burney, J., Burke, M., Schlenker, W., 2018. Estimating global agricultural effects of geoengineering using volcanic eruptions. Nature 560 (7719), 480–483. https://doi.org/10.1038/s41586-018-0417-3.

Qin, W., Liang, S., 2000. Plane-parallel canopy radiation transfer modeling: recent advances and future directions. Remote Sens. Rev. 18 (2–4), 281–305. https://doi.org/10.1080/02757250009532393.

Rap, A., Scott, C.E., Reddington, C.L., Mercado, L., Ellis, R.J., Garraway, S., et al., 2018. Enhanced global primary production by biogenic aerosol via diffuse radiation fertilization. Nat. Geosci. 11 (9), 640–644. https://doi.org/10.1038/s41561-018-0208-3.

Reichstein, M., Falge, E., Baldocchi, D., Papale, D., Aubinet, M., Berbigier, P., et al., 2005. On the separation of net ecosystem exchange into assimilation and ecosystem respiration: review and improved algorithm. Glob. Change Biol. 11 (9), 1424–1439. https://doi.org/10.1111/j.1365-2486.2005.001002.x.

Roderick, M.L., Farquhar, G.D., Berry, S.L., Noble, I.R., 2001. On the direct effect of clouds and atmospheric particles on the productivity and structure of vegetation. Oecologia 129 (1), 21–30. https://doi.org/10.1007/s004420100760.

Ross, J., 2012. The Radiation Regime and Architecture of Plant Stands, Vol. 3. Springer Science & Business Media.

Saxton, K.E., Rawls, W.J., 2006. Soil water characteristic estimates by texture and organic matter for hydrologic solutions. Soil Sci. Soc. Am. J. 70 (5), 1569–1578. https://doi.org/10.2136/sssaj2005.0117.

Schmidt, K., Feingold, G., Pilewskie, P., Jiang, H., Coddington, O., Wendisch, M., 2009. Irradiance in polluted cumulus fields: measured and modeled cloud-aerosol effects. Geophys. Res. Lett. 36 (7).

Schmidt, K.S., Venema, V., Giuseppe, F.D., Scheirer, R., Wendisch, M., Pilewskie, P., 2007. Reproducing cloud microphysical and irradiance measurements using three 3D cloud generators. Q. J. R. Meteorol. Soc. J. Atmosp. Sci., Appl. Meteorol. Phys. Oceanogr. 133 (624), 765–780.

Shao, L., Li, G., Zhao, Q., Li, Y., Sun, Y., Wang, W., et al., 2020. The fertilization effect of global dimming on crop yields is not attributed to an improved light interception. Glob. Chang. Biol. 26 (3), 1697–1713. https://doi.org/10.1111/gcb.14822.

Silva-Perez, V., Furbank, R.T., Condon, A.G., Evans, J.R., 2017. Biochemical model of C (3) photosynthesis applied to wheat at different temperatures. Plant Cell Environ. 40 (8), 1552–1564. https://doi.org/10.1111/pce.12953.

Slattery, R.A., Walker, B.J., Weber, A.P.M., Ort, D.R., 2018. The impacts of fluctuating light on crop performance. Plant Physiol. 176 (2), 990–1003. https://doi.org/10.1104/pp.17.01234.

Still, C.J., Riley, W.J., Biraud, S.C., Noone, D.C., Buenning, N.H., Randerson, J.T., et al., 2009. Influence of clouds and diffuse radiation on ecosystem-atmosphere CO2 and CO18O exchanges. J. Geophys. Res.: Biogeosci. 114 (G1). https://doi.org/10.1029/2007jg000675.

Strada, S., Unger, N., Yue, X., 2015. Observed aerosol-induced radiative effect on plant productivity in the eastern United States. Atmos. Environ. 122, 463–476. https://doi.org/10.1016/j.atmosenv.2015.09.051.

Tijhuis, M., van Stratum, B.J., Veerman, M.A., van Heerwaarden, C.C., 2023. An efficient parameterization for surface shortwave 3D radiative effects in large-eddy simulations of shallow cumulus clouds. J. Adv. Model. Earth Syst. 15 (1) e2022MS003262.

Tramontana, G., Migliavacca, M., Jung, M., Reichstein, M., Keenan, T.F., Camps-Valls, G., et al., 2020. Partitioning net carbon dioxide fluxes into photosynthesis and respiration using neural networks. Glob. Chang. Biol. 26 (9), 5235–5253. https://doi.org/10.1111/gcb.15203.

Urban, O., JanouŠ, D., Acosta, M., CzernÝ, R., MarkovÁ, I., NavrÁTil, M., et al., 2006. Ecophysiological controls over the net ecosystem exchange of mountain spruce stand. Comparison of the response in direct vs. diffuse solar radiation. Glob. Chang. Biol. 13 (1), 157–168. https://doi.org/10.1111/j.1365-2486.2006.01265.x.

Urban, O., Klem, K., Ač, A., Havránková, K., Holišová, P., Navrátil, M., et al., 2012. Impact of clear and cloudy sky conditions on the vertical distribution of photosynthetic CO2 uptake within a spruce canopy. Funct. Ecol. 26 (1), 46–55.

Vilà-Guerau de Arellano, J., Ney, P., Hartogensis, O., de Boer, H., van Diepen, K., Emin, D., et al., 2020. CloudRoots: integration of advanced instrumental techniques and process modelling of sub-hourly and sub-kilometre land–atmosphere interactions. Biogeosciences 17 (17), 4375–4404. https://doi.org/10.5194/bg-17-4375-2020.

von Caemmerer, S., 2013. Steady-state models of photosynthesis. Plant Cell Environ. 36 (9), 1617–1630. https://doi.org/10.1111/pce.12098.

Walker, A.P., Beckerman, A.P., Gu, L., Kattge, J., Cernusak, L.A., Domingues, T.F., et al., 2014. The relationship of leaf photosynthetic traits - V cmax and J max - to leaf nitrogen, leaf phosphorus, and specific leaf area: a meta-analysis and modeling study. Ecol. Evol. 4 (16), 3218–3235. https://doi.org/10.1002/ece3.1173.

Wang, S., Ibrom, A., Bauer-Gottwein, P., Garcia, M., 2018. Incorporating diffuse radiation into a light use efficiency and evapotranspiration model: an 11-year study in a high latitude deciduous forest. Agric. For. Meteorol. 248, 479–493. https://doi.org/10.1016/j.agrformet.2017.10.023.

Williams, I.N., Riley, W.J., Kueppers, L.M., Biraud, S.C., Torn, M.S., 2016. Separating the effects of phenology and diffuse radiation on gross primary productivity in winter wheat. J. Geophys. Res.: Biogeosci. 121 (7), 1903–1915. https://doi.org/10.1002/2015jg003317.

Williams, M., Rastetter, E.B., Van der Pol, L., Shaver, G.R., 2014. Arctic canopy photosynthetic efficiency enhanced under diffuse light, linked to a reduction in the fraction of the canopy in deep shade. New. Phytol. 202 (4), 1267–1276. https://doi.org/10.1111/nph.12750.

Wohlfahrt, G., Gu, L., 2015. The many meanings of gross photosynthesis and their implication for photosynthesis research from leaf to globe. Plant Cell Environ. 38 (12), 2500–2507. https://doi.org/10.1111/pce.12569.

Zhang, M., Yu, G.-R., Zhuang, J., Gentry, R., Fu, Y.-L., Sun, X.-M., et al., 2011. Effects of cloudiness change on net ecosystem exchange, light use efficiency, and water use efficiency in typical ecosystems of China. Agric. For. Meteorol. 151 (7), 803–816. https://doi.org/10.1016/j.agrformet.2011.01.011.

Zhang, Z., Zhu, K., Fan, M., Wang, Q., Tan, Y., 2024. Diffuse fertilization effect in maize and soybean is driven by improved light use efficiency rather than by light absorption. J. Geophys. Res.: Biogeosci. 129 (3). https://doi.org/10.1029/2023jg007766.

Zhao, W., Ren, T.H., Huang, X.Y., Xu, Z., Zhou, Y.Z., Yin, C.L., et al., 2023. Leaf shape, planting density, and nitrogen application affect soybean yield by changing direct and diffuse light distribution in the canopy. Plant Physiol. Biochem. 204, 108071. https://doi.org/10.1016/j.plaphy.2023.108071.

Zhou, H., Yue, X., Lei, Y., Tian, C., Ma, Y., Cao, Y., 2021a. Aerosol radiative and climatic effects on ecosystem productivity and evapotranspiration. Curr. Opin. Environ. Sci. Health 19. https://doi.org/10.1016/j.coesh.2020.10.006.

Zhou, H., Yue, X., Lei, Y., Zhang, T., Tian, C., Ma, Y., Cao, Y., 2021b. Responses of gross primary productivity to diffuse radiation at global FLUXNET sites. Atmosp. Environ. 244. https://doi.org/10.1016/j.atmosenv.2020.117905.

Zhou, S., Yu, B., Huang, Y., Wang, G., 2014. The effect of vapor pressure deficit on water use efficiency at the subdaily time scale. Geophys. Res. Lett. 41 (14), 5005–5013.